

Targeted Pandemic Containment Through Identifying Local Contact Network Bottlenecks

Shenghao Yang^{*} Priyabrata Senapati[†] Di Wang[‡] Chris T. Bauch[§]
Kimon Fountoulakis[¶]

April 27, 2022

Abstract

Decision-making about pandemic mitigation often relies upon mathematical modelling. Models of contact networks are increasingly used for these purposes, and are often appropriate for infections that spread from person to person. Real-world human contact networks are rich in structural features that influence infection transmission, such as tightly-knit local communities that are weakly connected to one another. In this paper, we propose a new flow-based edge-betweenness centrality method for detecting bottleneck edges that connect communities in contact networks. In particular, we utilize convex optimization formulations based on the idea of diffusion with p -norm network flow. Using mathematical models of COVID-19 transmission through real network data at both individual and county levels, we demonstrate that targeting bottleneck edges identified by the proposed method reduces the number of infected cases by up to 10% more than state-of-the-art edge-betweenness methods. Furthermore, we demonstrate empirically that the proposed method is orders of magnitude faster than existing methods.

1 Introduction

Mathematical and computer simulation models of COVID-19 transmission are being widely used during the COVID-19 pandemic for their ability to project future cases of infection under various possible scenarios for mitigation strategies [AEY⁺20, TFG20, KHG⁺20, VTD⁺20]. A significant subset of these models are network simulation models [BHR⁺20, RSK20, CDA⁺20]. In network models, the nodes of the network represent individuals or population centres, and the edges represent contacts through which SARS-CoV-2 (the virus that causes COVID-19) can spread. These models are often parameterized with data on demographic features, COVID-19 epidemiology, and population movement patterns [KYG⁺20, CST⁺20]. Network models are particularly relevant to COVID-19 control through physical distancing measures. These measures are effective but socially and economically costly. Therefore, physical distancing that targets the smallest number of nodes or edges of a contact network required to achieve public health goals is desirable.

The dynamics of infection transmission on networks are known to be very different from infection dynamics in homogeneously-mixing populations such as represented by compartmental epidemiological models [Het00, PBB⁺15, CPS10, PB09, KE05]. For instance, invasion thresholds can change in networks [CPS10] and spatial structure more generally can slow down the spread of the epidemic [RKW95, Bau05]. Moreover, the contact structure of networks suggests control strategies that can exploit its features. Previous models of infection control on networks have often

^{*}Department of Computer Science, University of Waterloo. Email: shenghao.yang@uwaterloo.ca.

[†]Department of Computer Science, University of Waterloo. Email: priyabrata.senapati@uwaterloo.ca.

[‡]Google Research, Mountain View, CA, USA. E-mail: wadi@google.com.

[§]Department of Computer Science, University of Waterloo. Email: cbauch@uwaterloo.ca.

[¶]Department of Computer Science, University of Waterloo. Email: kimon.fountoulakis@uwaterloo.ca.

concentrated on node-level characteristics such as node degree [Hol04, MH07, MvdDW13, WKB13]. For instance, models can be used to explore the impact of vaccination strategies that target highly connected nodes, or various different approaches to contact tracing [Hol04, MH07, MvdDW13, WKB13].

Earlier network modelling efforts focused on strategies for node-level characteristics because data on the structure of entire contact networks was once rare. However, such data is becoming increasingly available, making it possible to address strategies that target the larger-scale features of network structure such as how connected communities are to one another. It has been shown in simulated networks that vaccination targeted at individuals that bridge different communities in the network are more effective than targeting individuals with high node degree [SJ10]. These approaches detect important nodes and edges based on edge-betweenness measures. In particular, edge-betweenness is a measure of the influence an edge has over a diffusion process through the network (e.g., spread of infectious diseases). A classical example is that of shortest-path betweenness, which quantifies edge importance based on the assumption that information spreads only along shortest paths. However, it has been noted [SJ10] that this approach can overlook important connections in a network. For example, in Figure 1a we see that shortest-path betweenness only recognizes the shorter “bridge” in the middle, while completely neglecting the two longer, but still highly influential, side bridges. Random walk betweenness [New05]

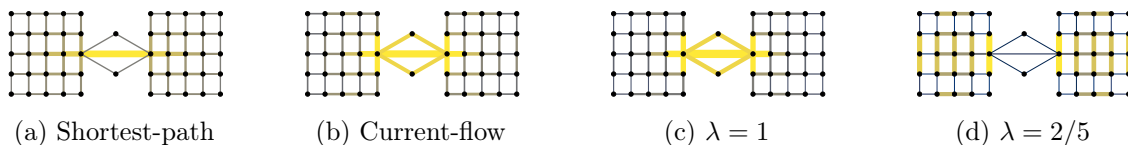


Figure 1: Edge-betweenness: color intensities and edge widths are chosen to reflect relative magnitude of betweenness measures.

fixes this problem of shortest-path betweenness by assuming that information spreads along random paths in the network while giving more weight to shorter paths. It is also named current-flow betweenness [BF05] due to the relation to network electrical current flows. Figure 1b shows that edge-betweenness that takes into account all possible walks captures the relative importance of all bridges. However, we note that human movement in large networks tends to be local [LLDM09, JBP⁺15]. Thus, containing the spread of infectious diseases usually requires identification and control of contact bottlenecks at a local scale rather than global. For example, cutting off all three bridges in Figure 1b would be terribly ineffective at slowing down the disease spread, if there was at least one infectious node in each of the two “square” clusters.

In this paper we develop a new edge-betweenness measure that we call λ -local flow betweenness, which is based purely on local diffusion in the network and offers a very flexible and localized quantification of edge importance. More precisely, when λ is small, λ -local flow betweenness tends to detect locally important edges as opposed to global bottlenecks that have little influence on local structure or processes. For example, Figure 1c shows that when $\lambda = 1$, it detects the same global bottlenecks as found by current-flow betweenness, but when we shrink $\lambda = 2/5$, it detects locally important bottlenecks within each block as shown in Figure 1d. Removing these bottlenecks would reduce disease transmission even if the infection is initially present in both sides. The proposed definition of edge-betweenness is based on p -norm flow diffusion [YWF20]. This diffusion is defined as a convex optimization problem that models the phenomenon of diffusing mass from a given node to nearby nodes that have non-zero capacities. More details are given in Section 2. The origin of p -norm flow diffusion is in local graph clustering methods. Because of this, the proposed edge-betweenness method induces locality and clustering biases, which we discuss in Sub-section 2.1. These inductive biases are crucial to the good performance of the proposed methods. Details are provided in Section 3.

We demonstrate that λ -local flow betweenness gives rise to better intervention strategies on all real datasets that we tested, and we discuss in detail why it is a more suitable measure for identifying disease transmission bottlenecks. We conduct exhaustive simulations and the

conclusions we draw from all experiments are consistent.

2 Network centrality based on local diffusion

In this section we define λ -local flow betweenness and determine its computational complexity. λ -local flow betweenness relies on p -norm flow diffusion [YWF20], which is used to solve the local graph clustering problem [FGM17]. There exist spectral [ST13, ACL06, ZLM13, AP09, FRKS⁺17] and combinatorial [AL08, OZ14, FLGM20, FGM17, WFH⁺17] local graph clustering methods. However, p -norm flow diffusion is as simple and as fast as spectral methods, but it has better conductance guarantees in theory and in practice. Moreover, p -norm diffusion requires less parameter tuning than combinatorial methods. For these reasons, we use it to define our edge-betweenness.

Given an undirected graph $G = (V, E)$ and signed incidence matrix B^1 using arbitrary orientation, we follow [YWF20] and define a diffusion process on G as the following convex optimization problem:

$$\text{minimize } \|f\|_p \quad \text{subject to } B^\top f + \Delta \leq T, \quad (1)$$

where $\Delta, T \in \mathbb{R}^{|V|}$ specify the amount of initial mass and sink capacity at each node, respectively, and $f \in \mathbb{R}^{|E|}$ are edge flow variables. The vector $B^\top f + \Delta$ gives the amount of final mass at each node if we start with initial mass Δ on nodes and send the mass around according to flow routing f , and we call a flow feasible if the final mass at each node is at most its capacity. The objective of (1) is to find a feasible flow f_p^* having the minimum p -norm². Naturally, in a diffusion we start with Δ having high density, i.e., there is a large amount of initial mass concentrated on a small set of nodes, and the sink capacities enforce we spread the mass to get lower density.

To take into account all relevant diffusion processes that start from arbitrary nodes and arbitrary sink capacities, we consider Δ and T in (1) as random variables following a probability distribution \mathcal{P} , under which its expected optimal objective value is finite. For $p \in (1, \infty)$, we define, in the most general sense, the p -norm flow edge-betweenness for an edge e as

$$\mathcal{B}_p(e; \mathcal{P}) := \mathbb{E}_{(\Delta, T) \sim \mathcal{P}}[\|f_p^*(e)\|]. \quad (2)$$

Of course, the specific inductive biases of p -norm flow edge-betweenness depend on the distribution \mathcal{P} . For example, let \mathcal{U}_V denote the discrete uniform distribution on the set of one-hot vectors $\{\mathbb{1}_v : v \in V\}$, then one obtains the current-flow betweenness as a special case:

Theorem 1. *For an edge $e \in E$, the current-flow betweenness [BF05] $c_{CB}(e)$ normalized by $1/|V|^2$ satisfies $c_{CB}(e) = \mathcal{B}_2(e; \mathcal{U}_V \times \mathcal{U}_V) = \mathbb{E}_{\Delta \sim \mathcal{U}_V, T \sim \mathcal{U}_V}[\|f_2^*(e)\|]$.*

2.1 Inductive Biases of λ -local flow betweenness

In order to introduce locality and clustering bias in (2), we let $\Delta \sim \mathcal{U}_V$ and fix $T = \frac{d}{\lambda \cdot \text{vol}(G)}$ where d is the degree vector, $\text{vol}(G)$ equals the sum of degrees of all nodes in G , and $\lambda \in (0, 1)$. We call the resulting specialized p -norm flow edge-betweenness as λ -local flow betweenness, as the locality of edge flows is controlled by λ , which we state formally in the following.

Theorem 2 (adapted to our problem from [YWF20]). *For $T = \frac{d}{\lambda \cdot \text{vol}(G)}$ and any fixed realization $\Delta = \mathbb{1}_v$, the number of edges with nonzero flow crossing them is bounded by $\|f_p^*\|_0 < 2\lambda|E|$.*

When $p = 2$, for any fixed Δ and T , one can compute f_2^* up to ϵ -accuracy in time $\mathcal{O}(\lambda|E|\bar{d}^2 \log \frac{1}{\epsilon})$ where $\bar{d} < \max_{i \in V} d_i$ [YWF20]. Therefore, λ -local flow betweenness for all edges can be computed in time $\mathcal{O}(\lambda|V||E|\bar{d}^2 \log \frac{1}{\epsilon})$. For sparse networks when \bar{d} is constant, if

¹ $|E| \times |V|$ matrix where the row of edge (u, v) has two non-zero entries, -1 at column u and 1 at column v .

²In general, we use subscripts p, Δ, T and write $f_{p, \Delta, T}^*$ to indicate the dependence of optimal solution to input parameters. We drop Δ, T from the subscript when they are clear from context and simply write f_p^* .

we set $\lambda = \mathcal{O}(1/|V|) = \mathcal{O}(1/|E|)$, then the computation time reduces to $\mathcal{O}(|V| \log \frac{1}{\epsilon})$. Note that small λ is what we rely on to detect local contact bottlenecks. In Section 3 we demonstrate that computing λ -local flow betweenness can be several orders of magnitude faster than computing shortest-path or current-flow betweenness, while the intervention strategies based on it achieve better disease containment.

Besides locality, one can show that f_p^* induces a strong local graph clustering bias in sparse networks for appropriately chosen λ . This local graph clustering bias will play a crucial role in our experiment. Formally, we quantify how “well-knit” a cluster is by measuring its conductance³.

Theorem 3 (adapted to our problem from [YWF20]). *Fix $p \in (1, \infty)$, $T = \frac{d}{\lambda \cdot \text{vol}(G)}$, and $\Delta = \mathbb{1}_v$ for some node v . The optimal solution to the dual of problem (1) gives a cluster \tilde{C} such that the conductance $\phi(\tilde{C}) \leq \mathcal{O}(\alpha \cdot \phi(C)^{1-1/p})$ holds simultaneously for any subset C containing v , where $\alpha = \mathcal{O}(\frac{\lambda \text{vol}(G)}{d_v})$ and d_v is the degree of v . In particular, in sparse graphs when we set $\lambda = \mathcal{O}(\frac{1}{\text{vol}(G)})$, the guarantee becomes $\phi(\tilde{C}) \leq \mathcal{O}(\phi(C)^{1-1/p})$.*

3 Experiments

We compare the effectiveness of interventions for the control of COVID-19 transmission that target edges⁴ meeting certain criteria, based on λ -local flow (LF(λ)) betweenness against other network centrality measures. We compare the following techniques: 1) Uniform Intervention (UI): reduce all contacts (i.e., edge weights) by a fixed amount, 2) High Degree (HD) intervention: reduce only the contacts of high degree nodes; and two state-of-the-art betweenness measures, 3) and 4) Shortest-Path (SP) and Current-Flow (CF) interventions: reduce important contacts recognized by SP and CF betweenness, respectively. In the past, SP and CF betweenness have been applied to wide range of problems including cancer diagnosis [Ram17], immunization modelling [SJ10], power grid contingency analysis [JHC⁺10], terrorist networks analysis [CKS02]. Hence, they are ideal candidates for comparison purposes. We use two SEIR network models to predict how COVID-19 infections will spread: 1) an ordinary differential equation (ODE) model where each node corresponds to a population in which an SEIR epidemic is occurring that can spread between nodes according to the network’s adjacency matrix, 2) an agent-based model where each node corresponds to a person, and the infection is transmitted from one node to the next with a certain probability per timestep. Details about the models and their parameter tuning are given in the supplementary material. We present the most informative figures in this section. Additional figures appear in the supplementary.

3.1 Datasets

FB-county network [BCK⁺18, BB18]. This Facebook social network consists of 3142 counties (nodes). Two counties are connected with an edge if there exists strong social interaction between them as measured by Facebook interactions.

Wi-Fi hotspots Montreal network [HHE⁺15]. This network consists of 103425 nodes and 630893 edges. Public WIFI hotspot networks are commonly used as proxies of human contact networks for studying transmission of infection across a network of individuals [HHE⁺15, HSB⁺16]. Each individual user is a node and concurrent usage of the same hotspot is an edge.

Portland, Oregon network [EGK⁺04]. This network was generated from time use and census data for the city of Portland, Oregon. It has been widely used in infectious disease modelling [EGK⁺04, BaLBB⁺06, WKB13]. The network consists of 1.6 million nodes and 31 million edges. We also make use of a sub-sampled version of this dataset that has 10,000 nodes and 199,168 edges [WKB13].

³The conductance of a subset of nodes $S \subseteq V$ is defined as $\phi(S) := \frac{|\partial(S)|}{\min\{d(S), d(V \setminus S)\}}$, where $\partial(S) = \{(u, v) \in E : u \in S, v \notin S\}$ and $d(S)$ is the sum of degrees of all nodes in S .

⁴We reduce targeted contact edge weights by 90%, e.g., physical contact reduction is naturally modelled as edge weight reduction or deletion. For more experiments under other weight reduction settings, see appendix.

In Figure 2 we demonstrate the Network Community Profile (NCP), the degree distribution and epidemic curves without intervention. The NCP captures clustering pattern of a network, i.e., the lower the NCP is the better. Details about the NCP are given in the supplementary material. In Figure 2a we demonstrate that the datasets correspond to the three distinct NCP classifications from [LLDM09, JBP⁺15]. In particular, FB-county has a downward sloping NCP, i.e., conductance decreases as size increases, Wi-Fi Montreal has roughly flat NCP, i.e., conductance does not change much as a function of size, and Portland, Oregon has upward sloping NCP, i.e., conductance are small at small sizes and increases as the size increases. We will exploit the NCP structure to define the initially infected nodes in our experiments. In Figure 2b we illustrate the degree distribution for the datasets. Note that the degree distribution for Montreal WiFi is heavily concentrated around nodes with degree ≤ 2 , which is more than half of the nodes in the network. This will play crucial role in the analysis of our experiments later on in this section. In Figure 2c we show the percentage of total active COVID-19 cases (prevalence of infection) against time (in days).⁵

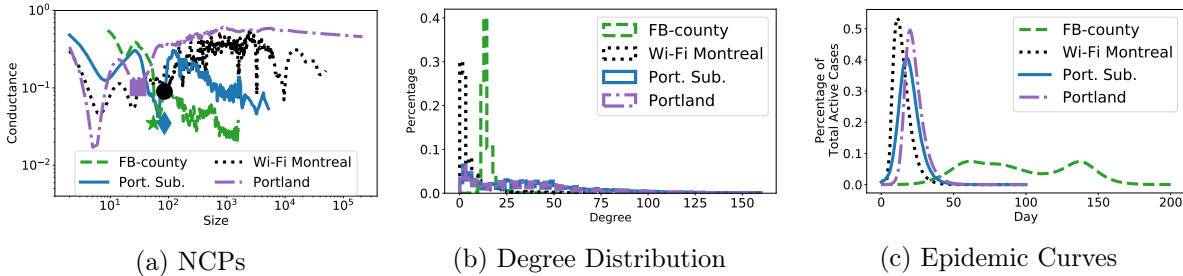


Figure 2: NCPs, degree distribution and epidemic curves (without intervention). The NCPs have been computed using [FLGM19, FGM18] based on the original paper [LLDM09]. The markers in the NCPs in Figure 2a correspond to clusters that we used to initialize the epidemic models for Figure 2c.

3.2 Computation time for λ -local flow betweenness

The time required for computing $LF(\lambda)$ betweenness depends linearly on λ . If the network is sparse and λ is proportional to $1/|V|$, then computing $LF(\lambda)$ to ϵ accuracy can be done in $O(|V| \log \frac{1}{\epsilon})$ time. For comparison, the computation time is at least $\mathcal{O}(|V|^2)$ for SP betweenness and $\mathcal{O}(|V|^2 \log |V|)$ for CF betweenness on sparse unweighted graphs⁶. In Figure 3 we compare the empirical computation times for SP, CF, and $LF(\lambda)$ betweenness on FB-county, Port. Sub., and Wi-Fi Montreal networks. All computations are carried out on a personal laptop with 32GB RAM and 2.9 GHz 6-Core Intel Core i9. We used NetworkX [HSS08] for computing SP and CF and implemented $LF(\lambda)$ computation in Julia. Observe that as λ becomes larger and $LF(\lambda)$ becomes more global, the time for computing $LF(\lambda)$ is similar to that of SP or CF. On the other hand, as λ becomes smaller, computing $LF(\lambda)$ gets several orders of magnitudes faster. This is crucial for scaling up our method to huge networks. For example, $LF(\lambda)$ is the only betweenness measure we are able to compute for the full Portland network.

⁵The curve for FB-county is very different from the other datasets because the data represent a nationwide geographic region and it takes a longer amount of time for the infection to spread from the Northeastern states to the rest of the country. This is also the reason that for FB-county the curves have multiple peaks, since there are multiple outbreaks in multiple cities as the disease progresses. In contrast, the other datasets correspond to outbreaks in a single urban centre that tend to unfold over weeks instead of months.

⁶For arbitrary unweighted graphs, the time is $\mathcal{O}(|V||E|)$ for SP betweenness [Bra01] and $\mathcal{O}(I(|V|) + |V||E| \log |V|)$ for CF betweenness [BF05], where $I(n)$ is the time to invert an $n \times n$ matrix.

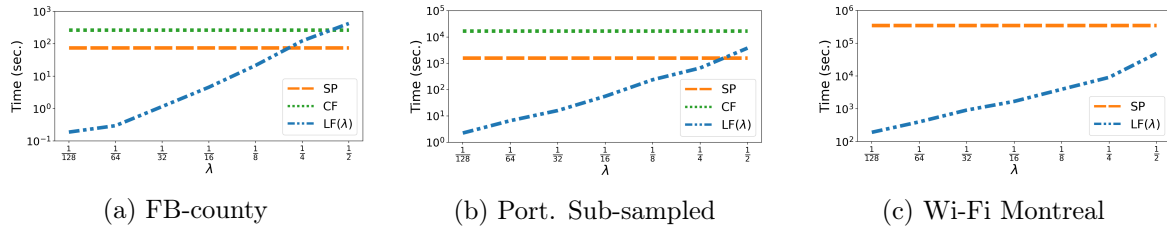


Figure 3: Comp. time for $LF(\lambda)$ betweenness. CF is omitted in (c) because it takes too long to finish.

3.3 Experiments for Facebook County network

We apply the ODE model to simulate the spread of COVID-19 on the FB-county network, since each node represents an entire county population. We assume that all county populations are initially susceptible and we pick infected counties for which we initialize 0.1% of the county population as infectious. We use three different ways to select initially infected counties to account for variations in where outbreaks could have started: (i) populated cosmopolitan cities (e.g., New York, Los Angeles), (ii) a tightly-knit cluster of 67 densely connected counties, highlighted in Figure 4a and also captured by the green star on the NCP in Figure 2a, and (iii) a random selection of 1% of all counties.

Figure 4b and 4c demonstrate the predicted epidemic curves and the final outbreak sizes during the epidemic under different levels of intervention for each method, for scenario (iii). (Results are similar for scenario (i) and (ii), see supplementary material.) Note that the epidemic curve using $LF(\lambda)$ intervention starts late, ends earlier, and has the lowest epidemic peak compared to the interventions based on SP or CF betweenness. Our results also show that for all three initial conditions and at all levels of intervention, $LF(\lambda)$ leads to the highest reduction in the epidemic size.

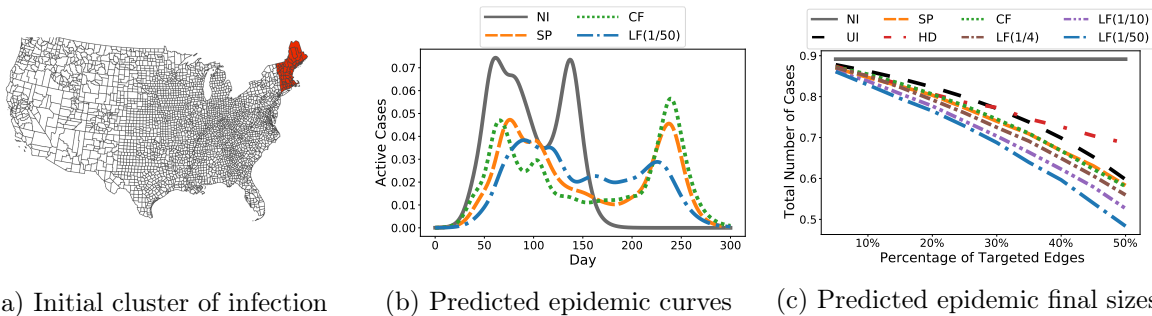


Figure 4: Simulation results for FB-county. Only four representative epidemic curves at 25% intervention level are drawn for cleaner visualization: e.g., we removed epidemic curves for HD due to its poor performance. See supplementary material for all curves and under different scenarios.

To study what makes $LF(\lambda)$ betweenness a much better indicator for local contact bottlenecks, we fix the intervention level at 25% of all edges and analyze the resulting networks. In Figure 5 we color each county according to how many edges incident to it have been targeted for contact reduction. We observe a significant difference in the patterns demonstrated by the three methods. Intervention based on SP results in scattered targets distributed over the country, whereas CF emphasizes the central east region, which consists of a large number of concentrated small counties. Both methods demonstrate a global pattern as being either globally dispersed or globally clustered. On the other hand, the targets of $LF(\lambda)$ betweenness form groups of small local clusters that spread across the country and loosely partition both east and west coasts into several smaller connected components. This observation is further supported in Figure 6a in which the NCP of the modified graph based on $LF(\lambda)$ has much lower conductance when cluster sizes are small. In Figure 6b we investigate this range by plotting the distribution of clusters of size less than

100 against conductance. Not surprisingly, the intervened network based on $LF(\lambda)$ betweenness contains more well-defined small clusters than the networks obtained from targeting high SP or CF betweenness, which has a more global focus. Finally, in Figure 6c we measure the percentage of out-link edges from the initial infected cluster (Figure 4a) that are targeted by different intervention strategies. Observe that the top 5% edges based on $LF(\lambda)$ betweenness already include all edges in the cut of the initial cluster. This explains why the epidemic curve under $LF(\lambda)$ starts rising later than others: because all out-link contacts have already been reduced. Note that $LF(\lambda)$ is un-supervised, i.e., it is not aware of the initially infected nodes, which demonstrates that local flow betweenness induces clustering bias, as promised by Theorem 3.

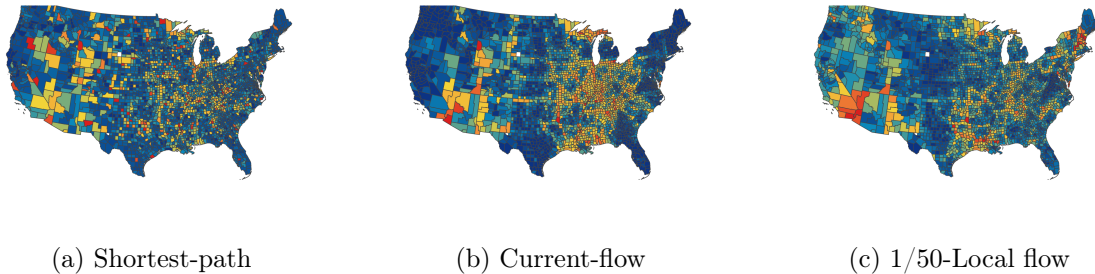


Figure 5: Distribution of target edges reflected by county-level colors: red means most incident edges are reduced (in edge weights), dark blue means few incident edges are reduced (in edge weights).

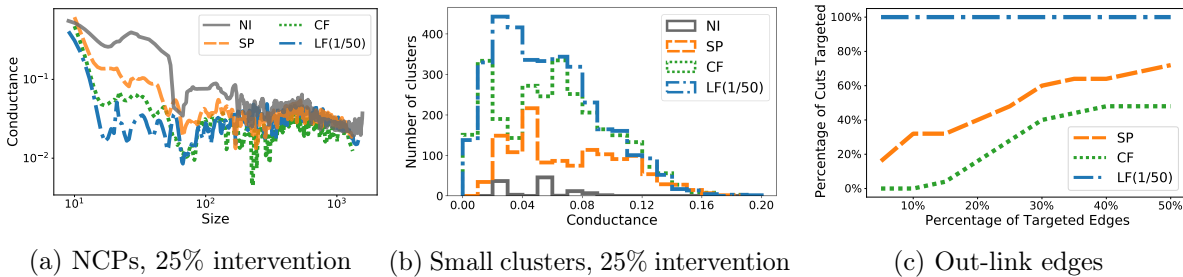


Figure 6: Network Community Profile (NCP), distribution of small-size clusters (having less than 100 nodes) by conductance, and percentage of targeted out-link edges from the initial cluster of infection, in the FB-county due to intervention based on different edge-betweenness measures.

3.4 Experiments for Wi-Fi Montreal network

We apply the agent-based SEIR network model to Wi-Fi Montreal, since each node now represents an individual person. We assign the initial state *Susceptible* to each person and then pick *Infectious* persons in two ways that cover very distinct scenarios: (i) as a group of 120 densely connected persons captured by the black circle on the NCP in Figure 2a, and (ii) as 0.1% of total population selected uniformly at random. We simulate the model until all state transitions reach equilibrium. The results for scenario (i) are shown in Figure 7 (see supplementary material for similar results for scenario (ii)), where in Figure 7b we also plot the peak of the epidemic curves at different intervention levels. Observe that in most cases, and in particular when targeting more than 20% of contact edges, $LF(\lambda)$ offers both significantly smaller epidemic size and a lower epidemic peak.

CF is omitted for this network due to prohibitive computation time⁷. We explain qualitatively what makes $LF(\lambda)$ work better than SP. As discussed earlier, more than half of the nodes in Wi-Fi Montreal have degree one or two (cf. Figure 2b), perhaps because these nodes represent

⁷Computing SP betweenness for Wi-Fi Montreal takes more than four days, while computing CF betweenness would take $O(\log |V|)$ more time. As a comparison, computing $LF(\lambda)$ for $\lambda = 1/50$ was done under 10 minutes.

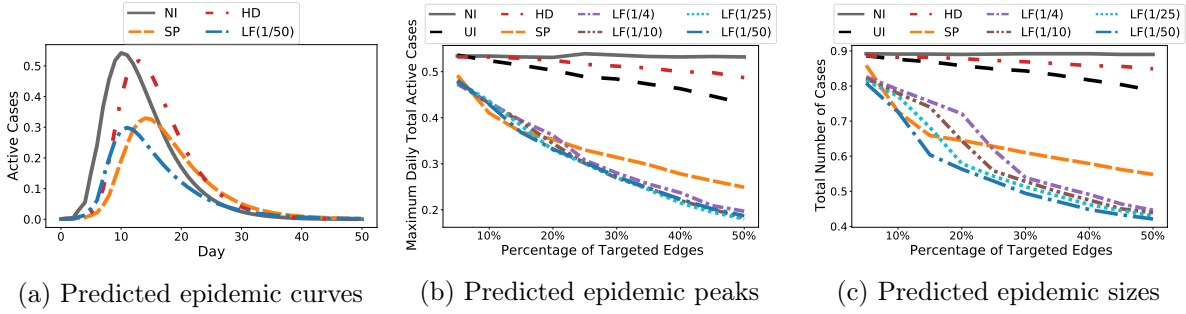


Figure 7: Simulation results for Wi-Fi Montreal. Only four representative epidemic curves (at 25% intervention level) are drawn for cleaner visualization. See supplementary for all curves and under different scenarios. The fluctuations in NI in (b) are due to probabilistic state transitions.

visitors. Hence, this network presents an extreme case where disconnecting all those small degree nodes could be a trivial yet effective solution. On the other hand, partitioning the entire graph into groups of clusters may not be as effective as it is for FB-county. In Figure 8 we demonstrate that $LF(\lambda)$ captures the degree irregularity in Wi-Fi Montreal and exploits this local information (i.e., many nodes have low degree). In particular, Figure 8a shows that intervention based on $LF(\lambda)$ does not necessarily generate more small clusters when the underlying graph has too many degree-one nodes. This is supported by Figure 8b where we see that the distribution of clusters of all sizes in the modified networks are similar. On the other hand, as shown in Figure 8c, where we measure how many singleton nodes are there if we were to remove all targeted edges, we notice that $LF(\lambda)$ separates far more singletons than SP does, thanks to its locality bias. The flexibility of incorporating local information (or going global if necessary, by controlling the value of λ) is what makes $LF(\lambda)$ versatile and effective.

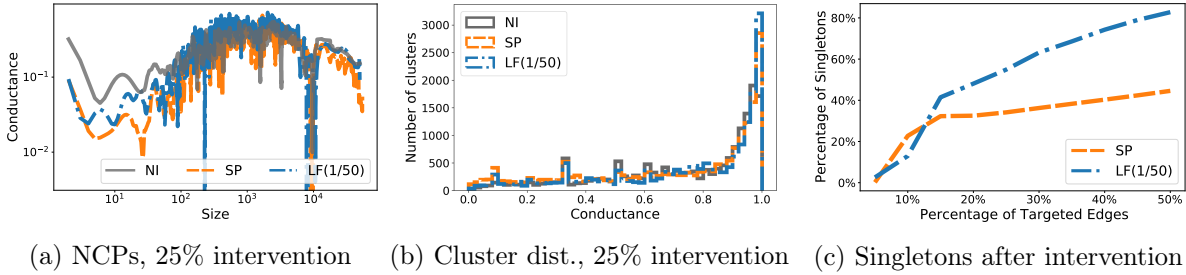


Figure 8: Locality bias of $LF(\lambda)$ for Wi-Fi Montreal is illustrated by the dramatic difference in (c).

3.5 Experiments for Portland, Oregon

We apply the agent-based model on both sub-sampled and full Portland contact networks. The sub-sampled network (Port. Sub.) is used first because the computation of both SP and CF betweenness measures do not scale to the full Portland dataset. We use Port. Sub. for comparison among different intervention methods and full Portland to demonstrate the effectiveness of $LF(\lambda)$ after scaling it up for large networks. We consider two initialization techniques for the model. First, we use well-connected clusters illustrated by the purple square and the blue diamond on the NCP in Figure 2a. Second, we select randomly 0.1% nodes from the entire population. For both datasets, the simulation results for both cluster and random initialization are shown in Figure 9. Observe that the results from different initialization schemes are very similar. In both scenarios, the smaller the λ , the smaller the total epidemic size. On the other hand, there is a trade-off between epidemic peak and epidemic size: on Port. Sub., $\lambda = 1/50$ gives the most reduction in epidemic size, whereas a slightly larger $\lambda = 1/10$ offers less reduction in total cases but gives a flatter epidemic curve (lower peak).

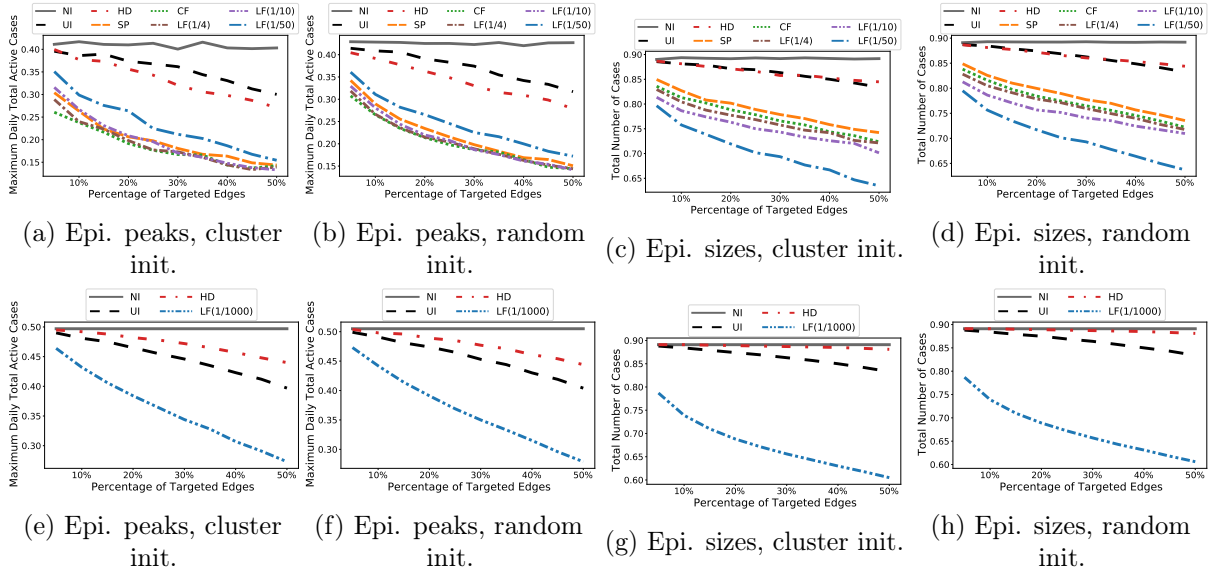


Figure 9: Simulation results for Port. Sub. (9a through 9d) and full Portland (9e through 9f). For Portland we used $\lambda = 1/1000$ for scalability. We average over 50 trials for random initialization.

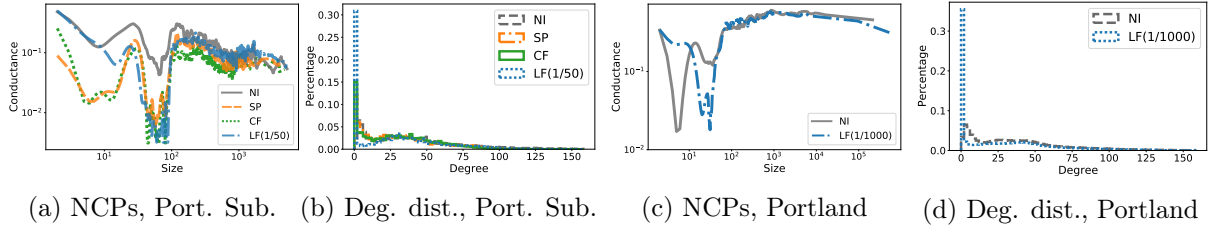


Figure 10: NCP and degree distribution for modified Port. Sub. and full Portland networks.

For Port. Sub., all three methods produce similar NCPs when cluster sizes are more than 30 as shown in Figure 9a. So NCP does not explain why LF(λ) leads to the most reduction in epidemic size. We further investigate the degree distributions in Figure 9b. Notice that more than 30% of all nodes in the LF(λ) intervention have degrees close to 0, which is more than double the amount created from SP or CF. This large amount of *almost-isolated* nodes (as they have degrees close to 0) makes it very difficult for an epidemic to spread across the entire population, and explains why intervention strategies based on LF(λ) leads to the mildest outbreak in terms of total infection. It also reveals that LF(λ) offers a better utilization of “budget” in the sense that most efforts in contact reduction are spent to create and isolate low degree nodes. Finally, for the full Portland network, while Figure 10c shows that there is a small difference in NCP, such difference is not as significant as it is demonstrated on the Facebook County network, and the major benefit of using LF(λ) on the full network still lies in the large amount of low degree nodes it created, as we show in Figure 10d.

4 Conclusion

Infection control methods that target features of network structure instead of features of individual nodes are increasingly feasible as empirical data on full contact networks becomes more abundant. At the same time, our network algorithms continue to improve. As we show here, λ local flow betweenness is orders of magnitude faster than competing methods, and physical distancing interventions based on λ local flow betweenness mitigate a simulated COVID-19 epidemic on realistic contact networks more effectively than other state-of-the-art approaches.

Potential Broader Impact

Large-scale pandemic interventions like school and workplace closure and other forms of physical (social) distancing can have enormous social and economic impacts. Highly optimized interventions that target key features of contact network architecture show promise to significantly reduce epidemic spread with minimal impact on the population, relative to “blunt instruments” like lockdown that impact the entire network. Our paper introduces a very fast method that can identify key network features and reduces COVID-19 spread more than competing state-of-the-art methods. However, implementing these methods in real time during a real-world epidemic would likely require large-scale digital monitoring of the population, which has negative implications for invasion of privacy and data protection.

Acknowledgements

The authors are grateful to Thomas Hladish for providing the Montreal WiFi network and to David F. Gleich for pointing to the Facebook County network. Kimon Fountoulakis would like to acknowledge NSERC for providing partial support for this work.

References

- [ACL06] R. Andersen, F. Chung, and K. Lang. Local graph partitioning using pagerank vectors. *FOCS '06 Proceedings of the 47th Annual IEEE Symposium on Foundations of Computer Science*, pages 475–486, 2006.
- [AEY⁺20] S. C Anderson, A. M Edwards, M. Yerlanov, N. Mulberry, J. Stockdale, S. A Iyaniwura, R. C Falcao, M. C Otterstatter, M. A Irvine, N. Z Janjua, et al. Estimating the impact of covid-19 control measures using a bayesian model of physical distancing. *medRxiv*, 2020.
- [AL08] R. Andersen and K. J. Lang. An algorithm for improving graph partitions. *Proceedings of the nineteenth annual ACM-SIAM symposium on Discrete algorithms*, pages 651–660, 2008.
- [AM92] R. M. Anderson and R. M. May. *Infectious diseases of humans: dynamics and control*. Oxford university press, 1992.
- [AMCyP⁺20] A. Aleta, D. Martin-Corral, A. P. y Piontti, M. Ajelli, M. Litvinova, M. Chinazzi, N. E Dean, E. M Halloran, I. M Longini, S. Merler, et al. Modeling the impact of social distancing, testing, contact tracing and household quarantine on second-wave scenarios of the covid-19 epidemic. *medRxiv*, 2020.
- [AP09] R. Andersen and T. Peres. Finding sparse cuts locally using evolving sets. In *STOC 2009*, pages 235–244, 2009.
- [BaLBB⁺06] K Bisset, K. Atkins and C. L Barrett, R Beckman, S. Eubank, A. Marathe, M. Marathe, HS Mortveit, P. Stretz, and VA Kumar. Synthetic data products for societal infrastructures and proto-populations: Data set 1.0. Technical report, TR-06-006, Network Dynamics and Simulation, 2006.
- [Bau05] C. T Bauch. The spread of infectious diseases in spatially structured populations: an invasy pair approximation. *Mathematical Biosciences*, 198(2):217–237, 2005.
- [BB18] E. Badger and Q. Bui. How connected is your community to everywhere else in america? *The New York Times*, 2018.

- [BC12] F. Brauer and C. C. Chavez. *Mathematical models in population biology and epidemiology*, volume 2. Springer, 2012.
- [BCK⁺18] M. Bailey, R. Cao, T. Kuchler, J. Stroebel, and A. Wong. Social connectedness: Measurement, determinants, and effects. *Journal of Economic Perspectives*, 32(3):259–280, 2018.
- [BF05] U. Brandes and D. Fleischer. Centrality measures based on current flow. In Volker Diekert and Bruno Durand, editors, *STACS 2005*, pages 533–544, Berlin, Heidelberg, 2005. Springer Berlin Heidelberg.
- [BHR⁺20] P. Block, M. Hoffman, I. J Raabe, J. B. Dowd, C. Rahal, R. Kashyap, and M. C Mills. Social network-based distancing strategies to flatten the covid 19 curve in a post-lockdown world. *arXiv preprint arXiv:2004.07052*, 2020.
- [Bra01] U. Brandes. A faster algorithm for betweenness centrality. *The Journal of Mathematical Sociology*, 25(2):163–177, 2001.
- [CDA⁺20] M. Chinazzi, J. T Davis, M. Ajelli, C. Gioannini, M. Litvinova, S. Merler, A. P. y Piontti, K. Mu, L. Rossi, K. Sun, et al. The effect of travel restrictions on the spread of the 2019 novel coronavirus (covid-19) outbreak. *Science*, 368(6489):395–400, 2020.
- [CDS09] R. Connell, P. Dawson, and A. Skvortsov. Comparison of an agent-based model of disease propagation with the generalised sir epidemic model. Technical report, Defense Science and Technology Organization Victoria (Australia), 2009.
- [CKS02] T. Carpenter, G. Karakostas, and D. Shallcross. Practical issues and algorithms for analyzing terrorist networks 1. In *Proceedings of the Western Simulation MultiConference*, 2002.
- [CPS10] C. Castellano and R. Pastor-Satorras. Thresholds for epidemic spreading in networks. *Physical review letters*, 105(21):218701, 2010.
- [CST⁺20] H. F. Chan, A. Skali, B. Torgler, et al. A global dataset of human mobility. Technical report, Center for Research in Economics, Management and the Arts (CREMA), 2020.
- [EGK⁺04] S. Eubank, H. Guclu, VS A. Kumar, M. V Marathe, A. Srinivasan, Z. Toroczkai, and N. Wang. Modelling disease outbreaks in realistic urban social networks. *Nature*, 429(6988):180–184, 2004.
- [ERBG00] D. JD Earn, P. Rohani, B. M Bolker, and B. T Grenfell. A simple model for complex dynamical transitions in epidemics. *Science*, 287(5453):667–670, 2000.
- [FGM17] K. Fountoulakis, D. F. Gleich, and M. W. Mahoney. An optimization approach to locally-biased graph algorithms. *Proceedings of the IEEE*, 105(2):256–272, 2017.
- [FGM18] K. Fountoulakis, D. F. Gleich, and M. W. Mahoney. A short introduction to local graph clustering methods and software. Technical report, 2018. Preprint: arXiv:1810.07324.
- [Fin03] P. EM Fine. The interval between successive cases of an infectious disease. *American journal of epidemiology*, 158(11):1039–1047, 2003.
- [FLGM19] K. Fountoulakis, M. Liu, D. Gleich, and M. W. Mahoney. Localgraphclustering API. <https://github.com/kfoynt/LocalGraphClustering>, January 2019.

- [FLGM20] K. Fountoulakis, M. Liu, D. F. Gleich, and M. W. Mahoney. Flow-based algorithms for improving clusters: A unifying framework, software, and performance. Technical report, 2020. Preprint: arXiv:2004.09608.
- [FRKS⁺17] K. Fountoulakis, F. Roosta-Khorasani, J. Shun, X. Cheng, and M. W. Mahoney. Variational perspective on local graph clustering. *Mathematical Programming B*, pages 1–21, 2017.
- [GBB⁺06] V. Grimm, U. Berger, F. Bastiansen, S. Eliassen, V. Ginot, J. Giske, J. Goss-Custard, T. Grand, S. K Heinz, G. Huse, et al. A standard protocol for describing individual-based and agent-based models. *Ecological modelling*, 198(1-2):115–126, 2006.
- [GBD⁺10] V. Grimm, U. Berger, D. L DeAngelis, J G. Polhill, J. Giske, and S. F Railsback. The odd protocol: a review and first update. *Ecological modelling*, 221(23):2760–2768, 2010.
- [HBB⁺20] N. Hoertel, M. Blachier, C. Blanco, M. Olfson, M. Massetti, F. Limosin, and H. Leleu. Facing the covid-19 epidemic in nyc: a stochastic agent-based model of various intervention strategies. *medRxiv*, 2020.
- [HD19] J. Hackl and T. Dubernet. Epidemic spreading in urban areas using agent-based transportation models. *Future Internet*, 11(4):92, 2019.
- [Het00] H. W. Hethcote. The mathematics of infectious diseases. *SIAM Review*, 42(4):599–653, 2000.
- [HHE⁺15] A. G. Hoen, T. J. Hladish, R. M. Eggo, M Lenczner, J. S. Brownstein, and L. A. Meyers. Epidemic wave dynamics attributable to urban community structure: A theoretical characterization of disease transmission in a large network. *Journal of Medical Internet Research*, 17(7), 2015.
- [HK20] J. Hilton and M. J Keeling. Estimation of country-level basic reproductive ratios for novel coronavirus (covid-19) using synthetic contact matrices. *medRxiv*, 2020.
- [Hol04] P. Holme. Efficient local strategies for vaccination and network attack. *EPL (Europhysics Letters)*, 68(6):908, 2004.
- [HSB⁺16] J. L Herrera, R. Srinivasan, J. S Brownstein, A. P Galvani, and L. A. Meyers. Disease surveillance on complex social networks. *PLoS computational biology*, 12(7), 2016.
- [HSS08] A. A. Hagberg, D. A. Schult, and P. J. Swart. Exploring network structure, dynamics, and function using networkx. In Gaël Varoquaux, Travis Vaught, and Jarrod Millman, editors, *Proceedings of the 7th Python in Science Conference*, pages 11 – 15, Pasadena, CA USA, 2008.
- [JBP⁺15] L. G. S. Jeub, P. Balachandran, M. A. Porter, P. J. Mucha, and M. W. Mahoney. Think locally, act locally: Detection of small, medium-sized, and large communities in large networks. *Physical Review E*, 91:012821, 2015.
- [JHC⁺10] S. Jin, Z. Huang, Y. Chen, D. Chavarría-Miranda, J. Feo, and P. C. Wong. A novel application of parallel betweenness centrality to power grid contingency analysis. In *2010 IEEE International Symposium on Parallel Distributed Processing (IPDPS)*, pages 1–7, 2010.
- [KAB20] V. Karatayev, M. Anand, and C. T Bauch. The far side of the covid-19 epidemic curve: local re-openings based on globally coordinated triggers may work best. *medRxiv*, 2020.

- [KE05] M. J Keeling and K. TD Eames. Networks and epidemic models. *Journal of the Royal Society Interface*, 2(4):295–307, 2005.
- [KHG⁺20] M. J. Keeling, E. Hill, E. Gorsich, B. Penman, G. Guyver-Fletcher, A. Holmes, T. Leng, H. McKimm, M. Tamborrino, L. Dyson, et al. Predictions of covid-19 dynamics in the uk: short-term forecasting and analysis of potential exit strategies. *medRxiv*, 2020.
- [KYG⁺20] M. UG Kraemer, C. Yang, B. Gutierrez, C. Wu, B. Klein, D. M Pigott, P. L. du, N. R Faria, R. Li, W. P Hanage, et al. The effect of human mobility and control measures on the covid-19 epidemic in china. *Science*, 368(6490):493–497, 2020.
- [LGWSR20] Y. Liu, A. A Gayle, A. Wilder-Smith, and J. Rocklöv. The reproductive number of covid-19 is higher compared to sars coronavirus. *Journal of travel medicine*, 2020.
- [LLDM09] J. Leskovec, K.J. Lang, A. Dasgupta, and M.W. Mahoney. Community structure in large networks: Natural cluster sizes and the absence of large well-defined clusters. *Internet Mathematics*, 6(1):29–123, 2009.
- [ME06] J. Ma and D. JD Earn. Generality of the final size formula for an epidemic of a newly invading infectious disease. *Bulletin of mathematical biology*, 68(3):679–702, 2006.
- [MH07] J. C Miller and J. M Hyman. Effective vaccination strategies for realistic social networks. *Physica A: Statistical Mechanics and its Applications*, 386(2):780–785, 2007.
- [MvdDW13] J. Ma, P v. d. Driessche, and F. H Willeboordse. The importance of contact network topology for the success of vaccination strategies. *Journal of theoretical biology*, 325:12–21, 2013.
- [New05] M.E. J. Newman. A measure of betweenness centrality based on random walks. *Social Networks*, 27(1):39 – 54, 2005.
- [NKY⁺20] M Linton N, T. Kobayashi, Y. Yang, K. Hayashi, A. R Akhmetzhanov, S. Jung, B. Yuan, R. Kinoshita, and H. Nishiura. Incubation period and other epidemiological characteristics of 2019 novel coronavirus infections with right truncation: a statistical analysis of publicly available case data. *Journal of clinical medicine*, 9(2):538, 2020.
- [NLA20] H. Nishiura, N. M Linton, and A. R Akhmetzhanov. Serial interval of novel coronavirus (covid-19) infections. *International Journal of Infectious Diseases*, 2020.
- [OZ14] L. Orecchia and Z. A. Zhu. Flow-based algorithms for local graph clustering. In *Proceedings of the 25th Annual ACM-SIAM Symposium on Discrete Algorithms*, pages 1267–1286, 2014.
- [PB09] A. Perisic and C. T Bauch. Social contact networks and disease eradicability under voluntary vaccination. *PLoS Comput Biol*, 5(2):e1000280, 2009.
- [PBB⁺15] L. Pellis, F. Ball, S. Bansal, K. Eames, T. House, V. Isham, and P. Trapman. Eight challenges for network epidemic models. *Epidemics*, 10:58–62, 2015.
- [PD09] L. Perez and S. Dragicevic. An agent-based approach for modeling dynamics of contagious disease spread. *International Journal of Health Geographics*, 8(1):50, 2009.

- [Ram17] J. Ramasamy. *A Betweenness Centrality Guided Clustering Algorithm and Its Applications to Cancer Diagnosis*, pages 35–42. Springer, 01 2017.
- [RKW95] D. Rand, M. Keeling, and H. Wilson. Invasion, stability and evolution to criticality in spatially extended, artificial host—pathogen ecologies. *Proceedings of the Royal Society of London. Series B: Biological Sciences*, 259(1354):55–63, 1995.
- [RSK20] O. Reich, G. Shalev, and T. Kalvari. Modeling covid-19 on a network: super-spreaders, testing and containment. *medRxiv*, 2020.
- [SJ10] M. Salathé and J. H. Jones. Dynamics and control of diseases in networks with community structure. *PLOS Computational Biology*, 6(4):1–11, 04 2010.
- [SRKFM16] J. Shun, F. Roosta-Khorasani, K. Fountoulakis, and M. W. Mahoney. Parallel local graph clustering. *Proceedings of the VLDB Endowment*, 9(12):1041–1052, 2016.
- [ST13] D. A. Spielman and S. H. Teng. A local clustering algorithm for massive graphs and its application to nearly linear time graph partitioning. *SIAM Journal on Scientific Computing*, 42(1):1–26, 2013.
- [TFG20] A. Tuite, D. N Fisman, and A. L Greer. Mathematical modeling of covid-19 transmission and mitigation strategies in the population of ontario, canada. *medRxiv*, 2020.
- [VTD⁺20] A. Vespignani, H. Tian, C. Dye, J. O. Lloyd-Smith, R. M. Eggo, M. Shrestha, S. V. Scarpino, B. Gutierrez, M. UG. Kraemer, J. Wu, et al. Modelling covid-19. *Nature Reviews Physics*, pages 1–3, 2020.
- [WFH⁺17] D. Wang, K. Fountoulakis, M. Henzinger, M. W. Mahoney, and S. Rao. Capacity releasing diffusion for speed and locality. In *Proceedings of the 34th International Conference on Machine Learning*, volume 70, pages 3607–2017, 2017.
- [WKB13] C. R Wells, E. Y Klein, and C. T Bauch. Policy resistance undermines superspreader vaccination strategies for influenza. *PLoS computational biology*, 9(3), 2013.
- [YD20] D. Yao and R. Durrett. Epidemics on evolving graphs. *arXiv preprint arXiv:2003.08534*, 2020.
- [YWF20] S. Yang, D. Wang, and K. Fountoulakis. p -norm flow diffusion for local graph clustering. In *Proceedings of the 37th International Conference on Machine Learning*, 2020.
- [ZLM13] Z. A. Zhu, S. Lattanzi, and V. S. Mirrokni. A local algorithm for finding well-connected clusters. In *Proceedings of the 30th International Conference on Machine Learning*, pages 396–404, 2013.

Supplementary material

A SEIR models

Models of infectious disease transmission typically divide the population into compartments based on their infection status, such as susceptible (S), infectious (I) and removed/recovered (R) [BC12, AM92]. Individuals move between compartments at certain rates according to assumptions about transmission and disease progression, and the compartments depend on disease or intervention being studied. For instance, an SLIR model with a latent (L) compartment accounts for the stage between being infected and starting to infect others [AMCyP⁺20]. Ordinary differential equations are often used to model the transmission processes in a large, homogeneously mixing population and can approximate dynamics adequately for many situations [Het00, TFG20, ERBG00]. For other applications it may be desirable to account for stochastic effects or contact heterogeneities, in which case probabilistic models and/or network models are preferable [YD20, KAB20, CDS09, PD09]. Agent-based models are an important subclass where simulated agents evolve according to certain rules and transitions between states are typically described as a probabilistic process [GBB⁺06], and are being widely used in the COVID-19 pandemic [HBB⁺20]. These models can simulate fine-scale individual movement behaviour or epidemiological characteristics [PD09, HD19].

In this paper we use two different types of COVID-19 transmission models. Both assume an SEIR disease progression in the host where individuals are in one of four mutually exclusive compartments: susceptible to infection (S), infected but not yet infectious (E), infectious (I), and removed (R). The first model described below is based on a system of ordinary differential equations (ODEs) [Het00] while the second is an agent-based model [GBB⁺06, GBD⁺10, WKB13].

A.1 Ordinary Differential Equation SEIR Network Model

Our ODE network SEIR model assumes that the proportion of susceptible, exposed, infectious and removed individuals in each population evolves according to an SEIR ODE model, and that transmission between populations occur through a network that connects these populations at rates determined by the network structure (connectivity and edge weights) of the Facebook County network. We define the following compartments:

- $S_i(t)$: number of susceptible persons at time t in population i ,
- $E_i(t)$: number of exposed persons (infected but not yet infectious) at time t in population i ,
- $I_i(t)$: number of infectious persons at time t in population i ,
- $R_i(t)$: number of removed persons at time t in population i ,
- N_i : number of persons in population i (constant),

and the following parameters:

- A_{ji} : number of contacts through which individuals in population j can infect individuals in population i . A_{ji} captures edge weights in the network of populations,
- β : average transmission rate per unit time per contact,
- σ_i : average rate per unit time at which an individual transitions from the exposed stage to the infectious stage, in population i ,
- γ_i : average rate per unit time at which an individual transitions from the infectious stage to the removed stage, in population i ,

The corresponding ODE SEIR network model is

$$\begin{aligned}\frac{dS_i}{dt} &= -\beta \sum_j A_{ji} \frac{I_j}{N_j} S_i \\ \frac{dE_i}{dt} &= \beta \sum_j A_{ji} \frac{I_j}{N_j} S_i - \sigma_i E_i \\ \frac{dI_i}{dt} &= \sigma_i E_i - \gamma_i I_i \\ \frac{dR_i}{dt} &= \gamma_i I_i .\end{aligned}$$

For our simulations we assume $\sigma_i = \sigma$ and $\gamma_i = \gamma$ for all i .

A.2 Agent Based Model SEIR Network Model

To model infection spread in a network of individuals, we introduce an agent-based network SEIR simulation model [GBB⁺06, GBD⁺10, WKB13]. An individual can be placed into one of following four states: (1) Susceptible (can contract the infection given contact with an infected individual), (2) Exposed (contracted the infection, but not yet infectious), (3) Infectious (with or without symptoms), and (4) Removed (either dead or obtained immunity and hence cannot infect others). The number of Susceptible, Exposed, Infectious, Removed, and total individuals can be denoted as S , E , I , R , N , respectively. When an infectious individual passes the infection to a susceptible individual, the susceptible agent is activated. The algorithm allows us to keep track of the Exposed and Infectious agents over time. As the number of activated agents increases so does the computational expense. We assumed that all edges have the same weight.

The total number of individuals within each of these disease states is given as:

- $S(t)$: number of susceptible persons at time t ,
- $E(t)$: number of exposed persons (infected but not yet infectious) at time t ,
- $I(t)$: number of infectious persons at time t ,
- $R(t)$: number of removed persons at time t ,
- N : number of persons in the population (constant),

and the parameters are:

- β : transmission probability along a network edge, per unit time,
- σ : probability that a person transitions from exposed to infectious, per unit time,
- γ : probability that a person transitions from infectious to removed, per unit time,

Each timestep in the discrete-time simulation corresponds to one day. The corresponding algorithm is as follows

1. Loop over all nodes (each node is a person) for each time step. For each node, the following may happen
 - If a person is in state S , then each infected neighbouring person has a probability β of infecting him/her, in which case the susceptible person moves from state $S \rightarrow E$.
 - If a person is in state E , s/he becomes infectious with probability σ and the status changes from $E \rightarrow I$.
 - If a person is in state I , s/he recovers with probability γ and the status changes from $I \rightarrow R$.
2. Update status of each person according to the events the person went through.
3. Repeat the steps for desired number of time steps.

A.3 COVID-19 model parameterization

We set the average duration of the latent period $1/\sigma = 2.5$ days and the average duration of the infectious period $1/\gamma = 5$ days based on epidemiological data on COVID-19 serial interval and incubation period [NLA20, NKY⁺20]. (We note that the latent and infectious periods do not correspond to the incubation period and duration of illness [Fin03].) We assumed a basic reproduction number $R_0 = 2.5$ for COVID-19 [LGWSR20, HK20]. We use the same values of σ , γ , and R_0 for both models. Calibration of the differential equation SEIR model for the Facebook County network and the agent-based SEIR model for the Wi-Fi Montreal and Portland networks required calibrating the value of β . In the agent-based network model, β is simply the transmission probability per edge per timestep. In the differential equation model, β is the coefficient of transmission in front of the adjacency matrix A_{ji} . In order to ensure comparability between these two model outputs, we calibrated their respective β values to obtain the outcome that 89% of the population eventually becomes infected in the absence of any interventions, in both models (i.e., $\lim_{t \rightarrow \infty} \sum_i R_i/N_i = 0.89$). This percentage was based on the SEIR epidemic final size formula $Z = 1 - \exp(-ZR_0)$ where Z is the final size [ME06], and our assumption that $R_0 = 2.5$. We modelled edge weight reduction due to interventions by reducing β values on the targeted edges accordingly.

B Missing proofs

B.1 Proof of Theorem 1

Fix $p = 2$, $\Delta = \mathbb{1}_s$ and $T = \mathbb{1}_t$ for some $s, t \in V$. Then the p -norm flow diffusion optimization problem

$$\text{minimize } \|f\|_p \quad \text{subject to } B^\top f + \Delta \leq T,$$

becomes

$$\text{minimize } \|f\|_2 \quad \text{subject to } B^\top f + \mathbb{1}_s \leq \mathbb{1}_t,$$

or equivalently,

$$\text{minimize } \frac{1}{2} \|f\|_2^2 \quad \text{subject to } B^\top f + \mathbb{1}_s = \mathbb{1}_t. \quad (\text{B.1})$$

where the equality constraint in the above is due to the fact $\|\mathbb{1}_s\|_1 = \|\mathbb{1}_t\|_1$. Let f_{st} denote the optimal solution of (B.1). Then by the optimality condition of (B.1), f_{st} satisfies, for some $y \in \mathbb{R}^{|V|}$,

$$f_{st} + By = 0, \quad (\text{B.2})$$

$$-B^\top f_{st} = \mathbb{1}_s - \mathbb{1}_t. \quad (\text{B.3})$$

Pre-multiply both sides of (B.2) by B^\top , and substitute (B.3), we have

$$Ly = B^\top By = -B^\top f_{st} = \mathbb{1}_s - \mathbb{1}_t, \quad (\text{B.4})$$

where L is the Laplacian matrix of G . Notice that (B.4) is exactly the Laplacian linear system that defines the absolute potentials y of a unique st -current τ_{st} (e.g., see Lemma 3 in [BF05]), where $\tau(e) = y(u) - y(v)$ for $e = (u, v) \in E$. Now, the relations between f_{st} and y are given by (B.3), i.e.,

$$f_{st}(e) = y(v) - y(u), \quad \text{for } e = (u, v) \in E.$$

Therefore $f_{st}(e) = -\tau_{st}(e)$ for all e . Moreover, if $s = t$, then simply $f_{st}(e) = 0$ for all e . It follows that

$$\mathbb{E}_{\Delta \sim \mathcal{U}_V, T \sim \mathcal{U}_V} [|f_2^*(e)|] = \frac{1}{|V|^2} \sum_{s, t \in V} |f_{st}(e)| = \frac{1}{|V|^2} \sum_{s, t \in V, s \neq t} |\tau_{st}(e)|,$$

which is exactly the current-flow betweenness [BF05] normalized by $1/|V|^2$.

B.2 Proofs of Theorem 2 and Theorem 3

Theorem 2 comes directly from Lemma 1 in [YWF20]. Theorem 3 is a straightforward application of Theorem 2 in [YWF20] to our setting.

C Network Community Profile

In the seminal papers [LLDM09, JBP⁺15] the authors studied how clustering structure of social networks changes as the size of the clusters increases. In particular, the NCP [LLDM09, JBP⁺15] function is defined as:

$$\Phi(k) := \min_{S \subset V} \phi(S) \quad \text{subject to: } |S| = k.$$

The NCP function takes as input the size k and asks for the minimum conductance that can be found in the graph such that the set S has size k . The NCP can be used to calculate the clustering resolution profile of the network as the size of the set increases. Based on the NCP, many real-world networks can be classified into three distinct cases according to their “size-resolved community structure”, (i) the best small communities have lower conductance than the best large communities (upward slopping NCP), (ii) the best small communities have comparable conductance to the best medium-sized and large communities (flat NCP), and (iii) the best small communities have higher conductance than the best large groups (downward slopping NCP). Computing the NCP function is NP-hard and it cannot be computed exactly, however, in [LLDM09, JBP⁺15] the authors have shown that it can be approximated (empirically) using local graph clustering algorithms [FGM17, WFH⁺17, FRKS⁺17, SRKFM16].

D More details about the datasets

FB-county network [BCK⁺18, BB18]. This Facebook social network consists of 3100 counties (nodes) and 22138 edges. Two counties are connected with an edge if there exists strong social interaction between them as measured by Facebook interactions. In this report, out of all the edges we keep only those that correspond to counties less than 500 miles apart. The resulting graph is still a connected graph. The post-processed graph maintains the structural properties that are discussed in the original article and paper [BCK⁺18, BB18], that is, social interaction tends to happen mostly among nearby counties.

Wi-Fi hotspots Montreal network [HHE⁺15]. This is a public WIFI hotspot network which we interpret as a contact network. WIFI networks are commonly used as proxies of human contact networks for studying transmission of infection across a network of individuals [HHE⁺15, HSB⁺16] This particular network is by Île Sans Fil (ISF), a not-for-profit organization established in 2004 in Montreal, Canada, that operates a system of public internet hotspots. Each individual user is a node and concurrent usage of the same hotspot is an edge. We use the post-processed network by [HHE⁺15], which consists of 103425 nodes and 630893 edges.

Portland, Oregon network [EGK⁺04]. This synthetic network was generated from time use and census data for the city of Portland, Oregon. It has also been widely used in infectious disease modelling [EGK⁺04, BaLBB⁺06, WKB13]. The full dataset consists of 1.6 million nodes and 31 million edges. We also make use of a sub-sampled version of this dataset that has 10,000 nodes and 199,168 edges [WKB13]. The reason that we sub-sample the original network is because the SP and CF betweenness methods do not scale to the initial network.

E Complete simulation results for intervention strategies with 90% weight reduction on targeted edges

In this section we show complete simulation results for all four networks: Facebook County, Wi-Fi Montreal, Portland Sub-sampled, and Portland, including the plots that are omitted in the main

text due to page limit.

Predicted epidemic dynamics for intervention strategies that reduce 90% edge weights on targeted edges on the Facebook County network are shown in Figure 11. Note that targeting edges according to $\text{LF}(\lambda)$ betweenness leads to the most reduction in epidemic outbreak sizes for all initialization scenarios, and it consistently lowers the epidemic peaks by a large amount, which is more stable than other methods. For example, intervention based on the current-flow (CF) betweenness can give rise to very unstable epidemic peaks, as shown in Figure 11e when the epidemic starts from Los Angeles, California. Furthermore, observe that targeting high degree nodes can be less effective than uniformly reducing contacts throughout the network, as shown in Figure 11e and 11f.

Figure 12 demonstrates the results on the Wi-Fi Montreal network, where $\text{LF}(\lambda)$ is shown to be the most effective at reducing both epidemic peaks and total outbreak sizes.

The complete simulation results for both Portland Sub-sampled and full Portland networks, including the epidemic curves at 25% intervention level, are shown in Figure 13 and Figure 14. Overall, $\text{LF}(\lambda)$ still delivers the best outcome. The predicted epidemic results on Portland Sub-sampled demonstrates a trade-off in λ : a smaller $\lambda = 1/50$ yields the most reduction in total infections, and a larger $\lambda = 1/4$ or $\lambda = 1/10$ lowers the epidemic peaks more.

F Additional experiments for intervention strategies with 99% weight reduction on targeted edges

We carry out an additional complete set of experiments where the targeted edge weights are reduced by 99% in various intervention strategies. This can model, for example, situations where only emergency contacts are allowed over intervened contact channels in the network. Simulation results for this setting are shown in Figures 15, 16, 17, 18. Observe the results are very similar to the 90% weight reduction setting. On Facebook County, Wi-Fi Montreal, and full Portland networks, interventions based on $\text{LF}(\lambda)$ result in the largest reduction in both epidemic peaks and outbreak sizes. For the Portland Sub-sampled network, there is a trade-off among different λ choices, nonetheless, $\text{LF}(\lambda)$ gives the best overall epidemic control.

G Additional experiments on $\text{LF}(\lambda)$ with general p -norm for p larger than 2

Recall that $\text{LF}(\lambda)$ is a special case of the more general p -norm flow betweenness defined in the main text, where $p \in (1, \infty)$. Until now we have used $p = 2$ for $\text{LF}(\lambda)$ because of its computational efficiency, but we don't necessarily need to restrict ourselves to the case $p = 2$. Furthermore, Theorem 3 states that a larger $p > 2$ induces a stronger clustering bias. In this section, we experiment with using different p values in the definition of λ -local betweenness. In particular, we take $p = 4$ and compute the corresponding $\text{LF}(\lambda)$ betweenness, for $\lambda \in \{1/10, 1/50\}$. We pick $p = 4$ because, it has been empirically demonstrated in the local graph clustering settings [YWF20] that, $p = 4$ is large enough to produce a significantly stronger clustering bias than $p = 2$. The following empirical results demonstrate that this is indeed the case.

For each of the four datasets, we compare interventions that reduce 90% edge weights on targeted edges based on $\text{LF}(\lambda)$ for $p = 2$ and $p = 4$. The results are shown in Figures 19, 20, 21, 22. As demonstrated and discussed in the main text, clustering bias plays a major role in the efficacy of interventions on the Facebook County network. Therefore, as expected and also as shown in Figure 19, when $p = 4$ and $\lambda = 1/50$, $\text{LF}(\lambda)$ produces larger reduction (up to 5% of total population) in the total outbreak sizes, while maintaining a similar outbreak peak level (up to 0.5% difference). On the other hand, the Wi-Fi Montreal network is a special network where more than half of nodes have degree one or two, so clustering should not help at all. This is

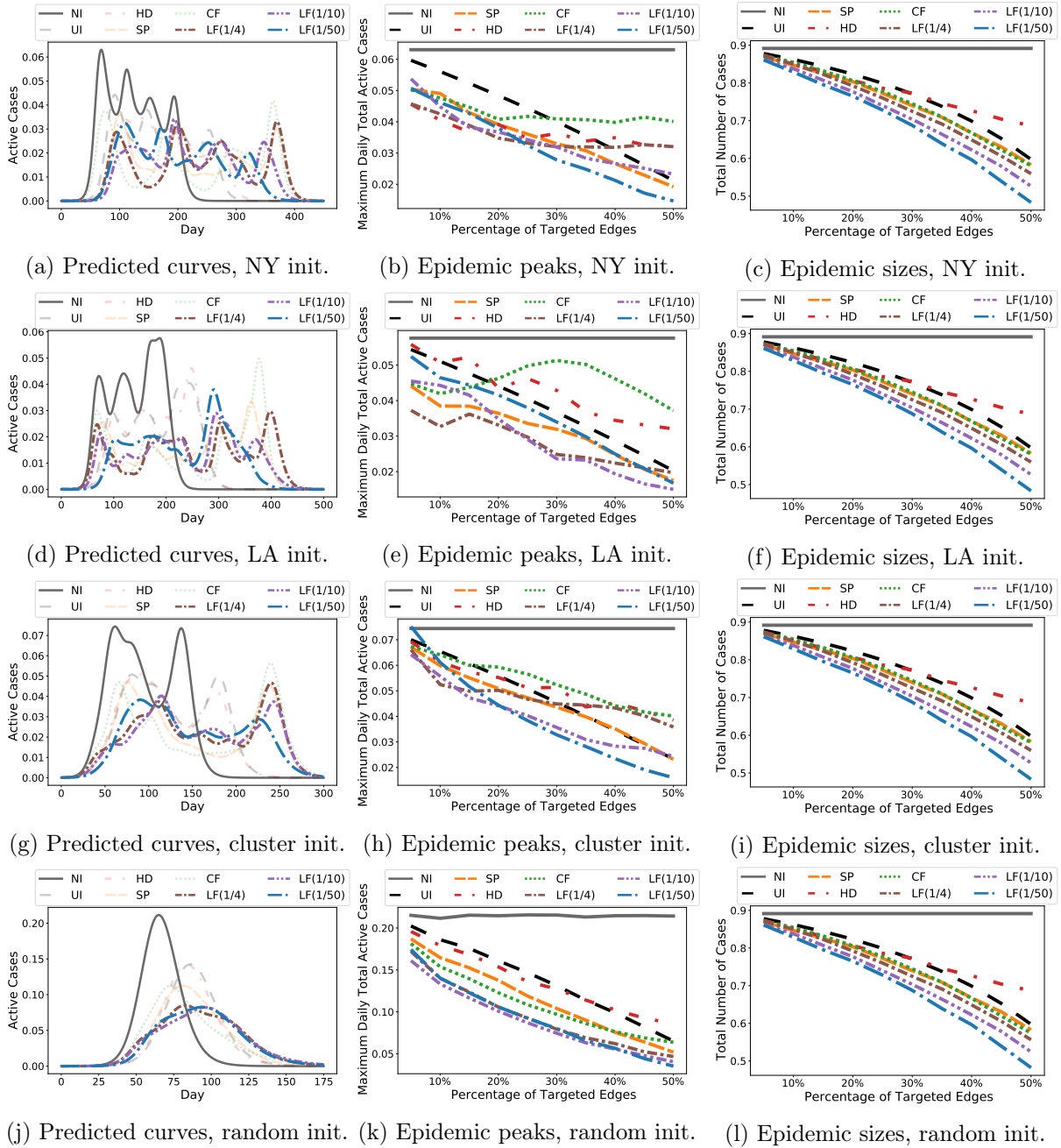


Figure 11: Simulation results for the Facebook County network when *reducing 90% of the weights* on targeted edges. We illustrate Predicted epidemic curves, epidemic peaks (i.e., maximum daily active cases), and outbreak sizes (i.e., total number of infections throughout the outbreak) for four different initialization scenarios. In Scenario 1, the epidemic starts from New York, New York; In Scenario 2, the epidemic starts from Los Angeles, California; In Scenario 3, the epidemic starts from a well-connected cluster of 67 counties; In Scenario 4, the epidemic starts from a random selection of 1% of all counties across the country. We plot all epidemic curves at 25% intervention level, and we highlight the original epidemic curve (i.e., no intervention) along with the top 3 curves that achieve the mildest outbreak sizes. We average over 50 trials for random initialization.

reflected in Figure 20, where for $\lambda = 1/50$, the results for $p = 2$ and $p = 4$ are almost identical⁸.

⁸For $\lambda = 1/10$, the poor performance of $p = 4$ shows that a stronger clustering bias can even be harmful for the star-like Wi-Fi Montreal network, since larger $\lambda = 1/10$ forces $LF(\lambda)$ to focus on the global clustering structure of the graph, which is not useful in this special case.

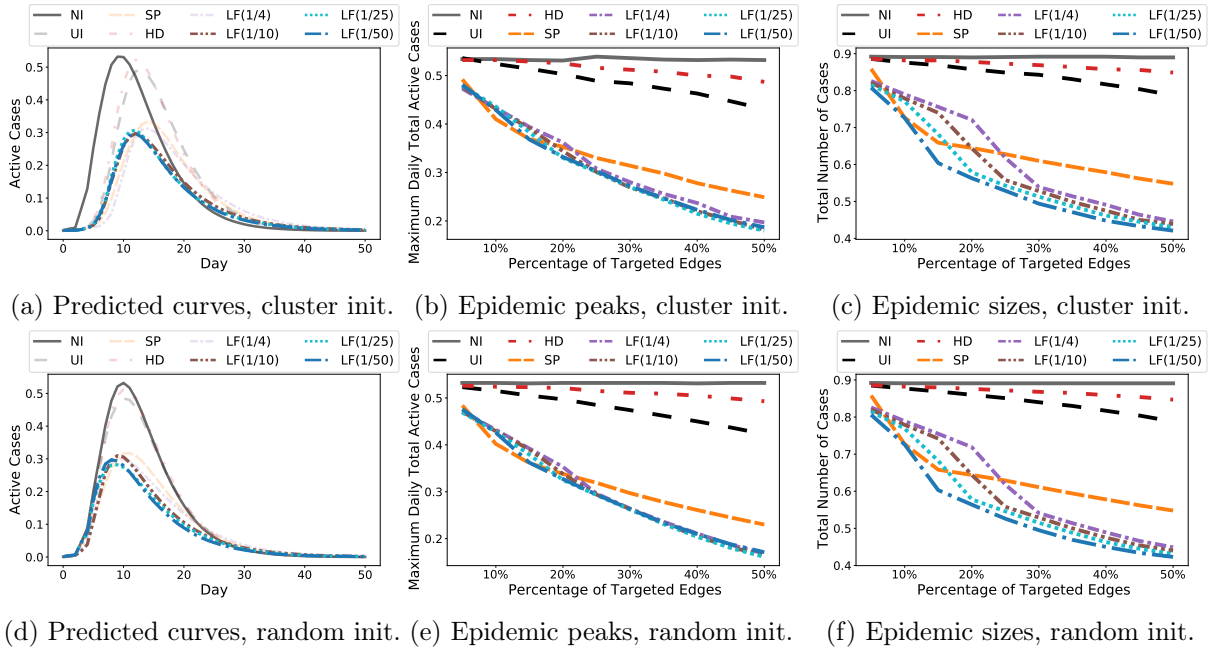


Figure 12: Simulation results for the Wi-Fi Montreal network when *reducing 90% of the weights* on targeted edges. We illustrate Predicted epidemic curves, epidemic peaks (i.e., maximum daily active cases), and outbreak sizes (i.e., total number of infections throughout the outbreak) for two different initialization scenarios. In Scenario 1, the epidemic starts from a well-connected cluster of 101 infected persons; In Scenario 2, the epidemic starts from a random selection of 0.1% of all population as initially infectious. We plot epidemic curves at 25% intervention level, and we highlight the original epidemic curve (i.e., no intervention) along with the top 3 curves that achieve the mildest outbreak sizes. We average over 50 trials for random initialization.

Finally, on the Portland Sub-sampled and full Portland, we see a trade-off between $p = 2$ and $p = 4$, that is, $p = 4$ does not always guarantee the largest reduction in both epidemic peak and outbreak size.

Our results in this section demonstrate that if local clusters of the graph play an important role in spreading a disease (e.g., the Facebook County network), then using $p = 4$ can significantly improve intervention results; otherwise, $p = 2$ would suffice.

H Node-betweenness extension

Even though our definition of p -norm flow betweenness naturally applies to edges due to its physical interpretation of expected optimal flow in a diffusion process, there is a straightforward extension to node-betweenness measures, by aggregating flows on all incident edges of a node, i.e.,

$$\mathcal{B}_p(v; \mathcal{P}) := \sum_{e \in E: v \in e} \mathcal{B}_p(e; \mathcal{P}).$$

For example, a special case of this node-betweenness measure when $\mathcal{P} = \mathcal{U}_V \times \mathcal{U}_V$ is the node current-flow betweenness [BF05].

In the rest of this section we show simulation results for intervention strategies that target important nodes based on node-betweenness measures. We compare node λ -local flow (LF(λ)) betweenness with a baseline method that targets High Degree (HD) nodes, and two node-betweenness measures, namely, Shortest-Path (SP) and Current-Flow (CF). For each intervention method, we fix the number of intervened nodes, and we reduce edge weights by 90% on all edges incident to the targeted nodes. The results are shown in Figures 23, 24, 25, 26. Observe that the advantage of LF(λ) is even more pronounced in this setting. In particular, LF(λ) clearly

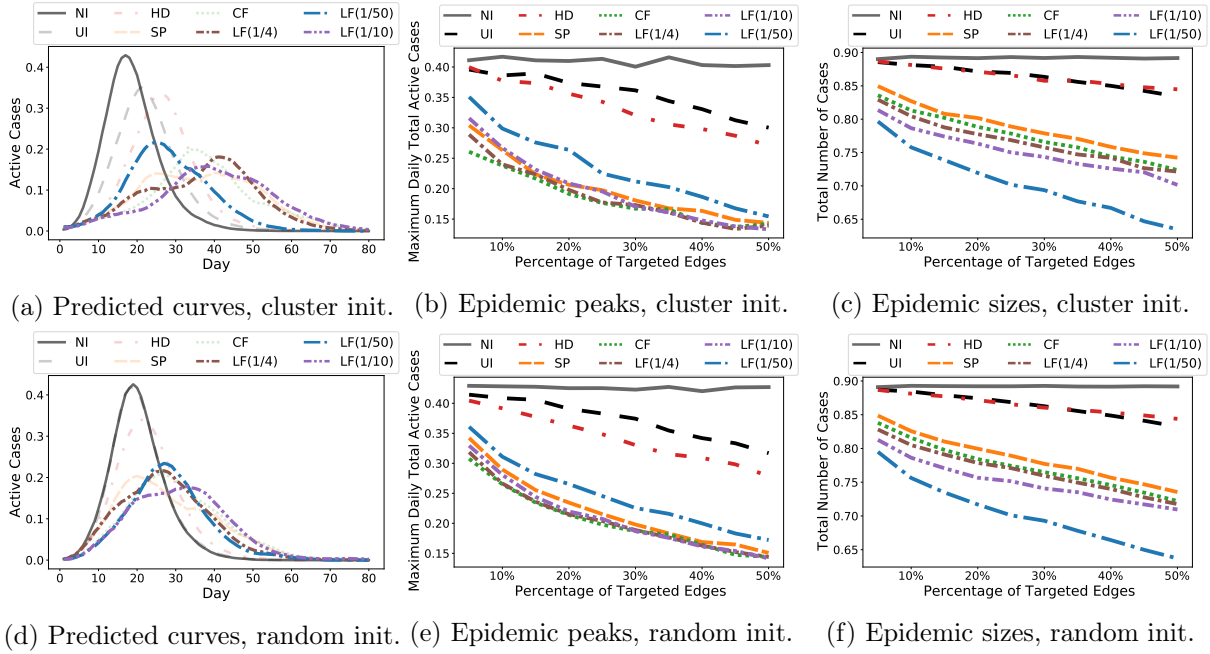
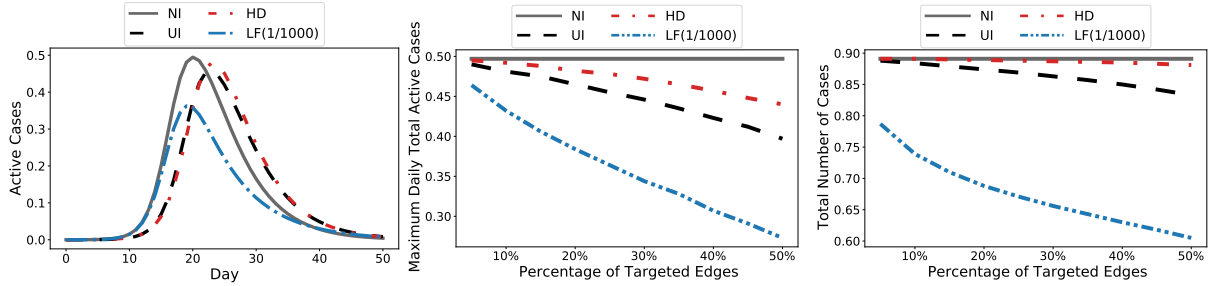


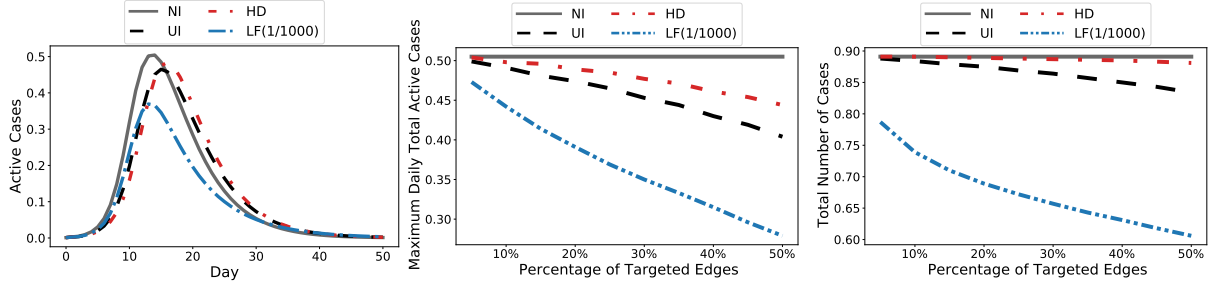
Figure 13: Simulation results for the Portland Sub-sampled network when *reducing 90% of the weights* on targeted edges. We illustrate Predicted epidemic curves, epidemic peaks (i.e., maximum daily active cases), and outbreak sizes (i.e., total number of infections throughout the outbreak) for two different initialization scenarios. In Scenario 1, the epidemic starts from a well-connected cluster of 80 infected persons; In Scenario 2, the epidemic starts from a random selection of 0.1% of all population as initially infectious. We plot epidemic curves at 25% intervention level, and we highlight the original epidemic curve (i.e., no intervention) along with the top 3 curves that achieve the mildest outbreak sizes. We average over 50 trials for random initialization.

outperforms all other methods on the Facebook County network at reducing both the epidemic peak and the outbreak size. On the Wi-Fi Montreal and Portland Sub-sampled networks, all methods give similar results⁹, except that HD has a noticeably worse performance.

⁹The computation times for $LF(\lambda)$ are orders of magnitude faster, similar to what is presented in the main paper.



(a) Predicted curves, cluster init. (b) Epidemic peaks, cluster init. (c) Epidemic sizes, cluster init.



(d) Predicted curves, random init. (e) Epidemic peaks, random init. (f) Epidemic sizes, random init.

Figure 14: Simulation results for the full Portland network when *reducing 90% of the weights* on targeted edges. We illustrate Predicted epidemic curves, epidemic peaks (i.e., maximum daily active cases), and outbreak sizes (i.e., total number of infections throughout the outbreak) for two different initialization scenarios. In Scenario 1, the epidemic starts from a well-connected cluster of 37 infected persons; In Scenario 2, the epidemic starts from a random selection of 0.1% of all population as initially infectious. We used $\lambda = 1/1000$ for scalability. The epidemic curves are drawn at 25% intervention level. We average over 50 trials for random initialization.

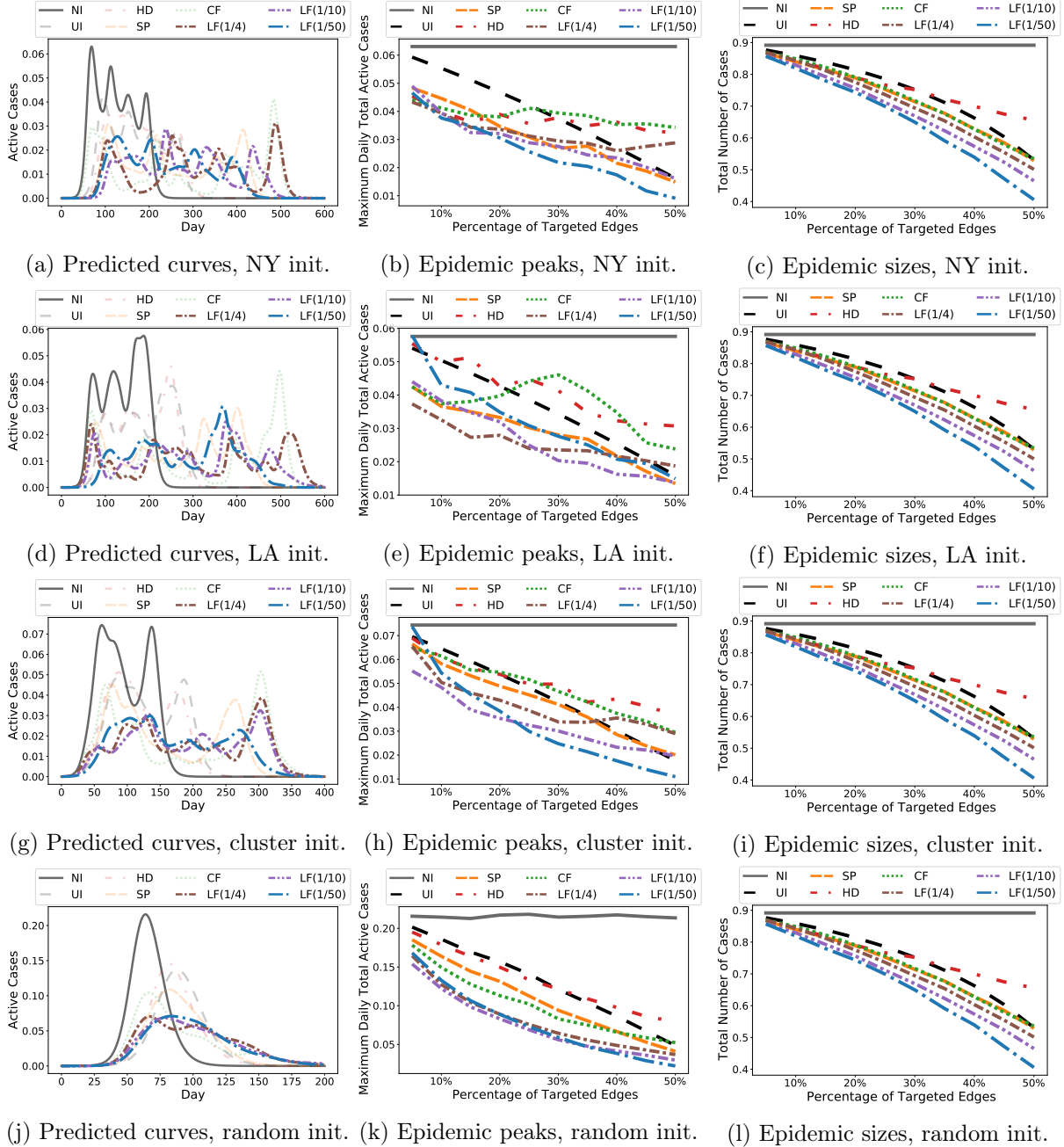


Figure 15: Simulation results for the Facebook County network when *reducing 99% of the weights* on targeted edges. We illustrate Predicted epidemic curves, epidemic peaks (i.e., maximum daily active cases), and outbreak sizes (i.e., total number of infections throughout the outbreak) for four different initialization scenarios. In Scenario 1, the epidemic starts from New York, New York; In Scenario 2, the epidemic starts from Los Angeles, California; In Scenario 3, the epidemic starts from a well-connected cluster of 67 counties; In Scenario 4, the epidemic starts from a random selection of 1% of all counties across the country. We plot all epidemic curves at 25% intervention level, and we highlight the original epidemic curve (i.e., no intervention) along with the top 3 curves that achieve the mildest outbreak sizes. We average over 50 trials for random initialization.

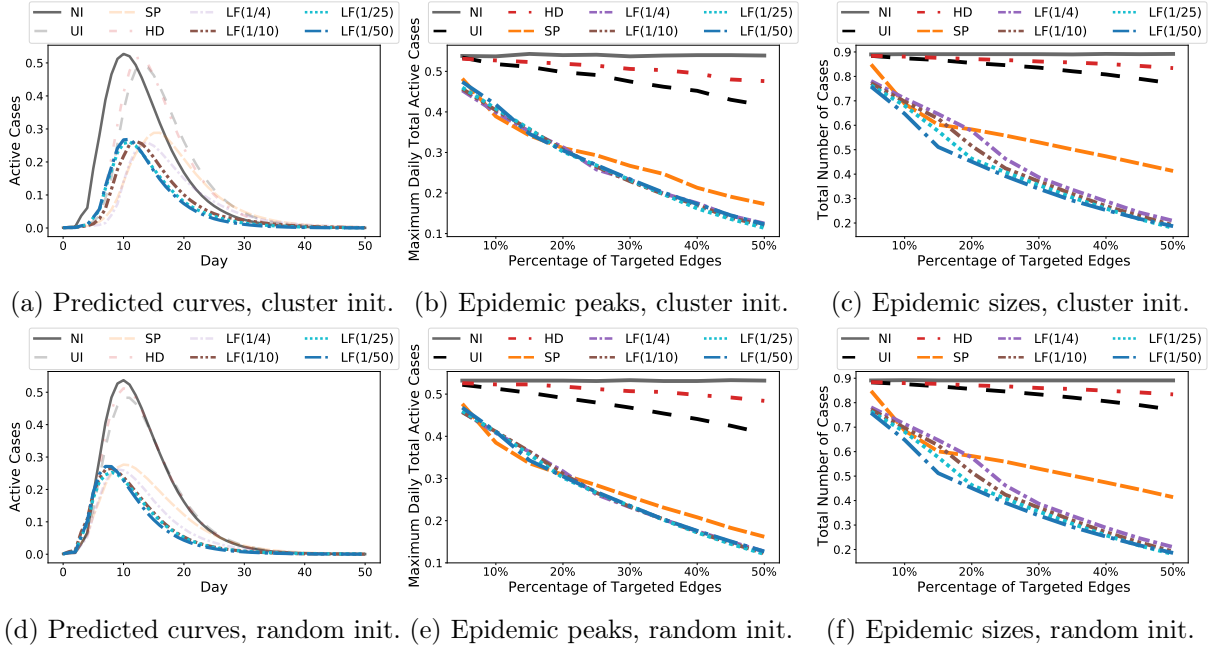


Figure 16: Simulation results for the Wi-Fi Montreal network when *reducing 99% of the weights* on targeted edges. We illustrate Predicted epidemic curves, epidemic peaks (i.e., maximum daily active cases), and outbreak sizes (i.e., total number of infections throughout the outbreak) for two different initialization scenarios. In Scenario 1, the epidemic starts from a well-connected cluster of 101 infected persons; In Scenario 2, the epidemic starts from a random selection of 0.1% of all population as initially infectious. We plot epidemic curves at 25% intervention level, and we highlight the original epidemic curve (i.e., no intervention) along with the top 3 curves that achieve the mildest outbreak sizes. We average over 50 trials for random initialization.

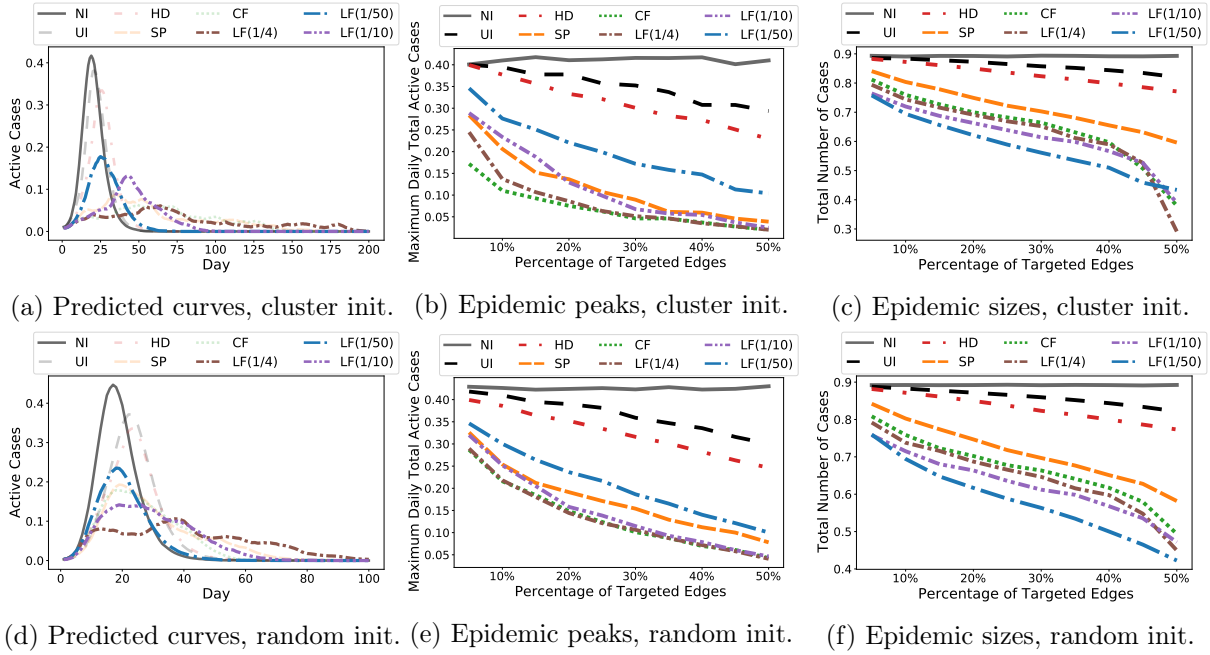
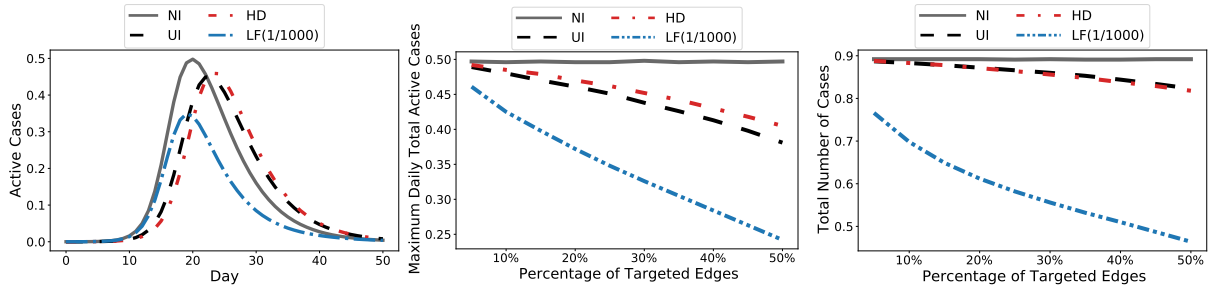
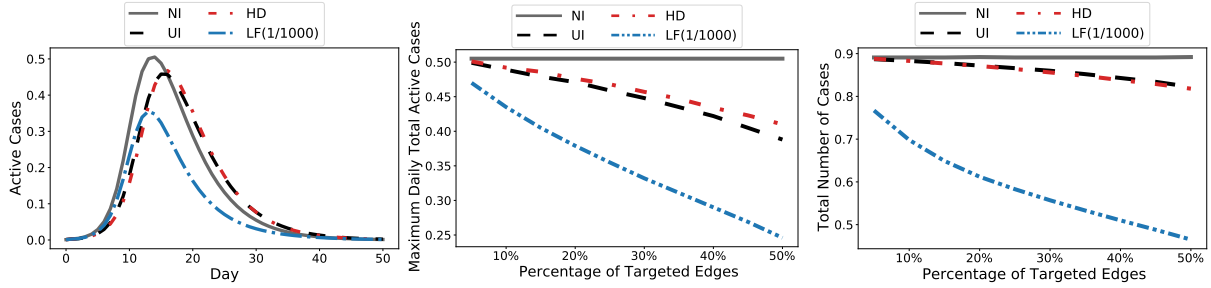


Figure 17: Simulation results for the Portland Sub-sampled network when *reducing 99% of the weights* on targeted edges. We illustrate Predicted epidemic curves, epidemic peaks (i.e., maximum daily active cases), and outbreak sizes (i.e., total number of infections throughout the outbreak) for two different initialization scenarios. In Scenario 1, the epidemic starts from a well-connected cluster of 80 infected persons; In Scenario 2, the epidemic starts from a random selection of 0.1% of all population as initially infectious. We plot epidemic curves at 25% intervention level, and we highlight the original epidemic curve (i.e., no intervention) along with the top 3 curves that achieve the mildest outbreak sizes. We average over 50 trials for random initialization.



(a) Predicted curves, cluster init. (b) Epidemic peaks, cluster init. (c) Epidemic sizes, cluster init.



(d) Predicted curves, random init. (e) Epidemic peaks, random init. (f) Epidemic sizes, random init.

Figure 18: Simulation results for the full Portland network when *reducing 99% of the weights* on targeted edges. We illustrate Predicted epidemic curves, epidemic peaks (i.e., maximum daily active cases), and outbreak sizes (i.e., total number of infections throughout the outbreak) for two different initialization scenarios. In Scenario 1, the epidemic starts from a well-connected cluster of 37 infected persons; In Scenario 2, the epidemic starts from a random selection of 0.1% of all population as initially infectious. We used $\lambda = 1/1000$ for scalability. The epidemic curves are drawn at 25% intervention level. We average over 50 trials for random initialization.

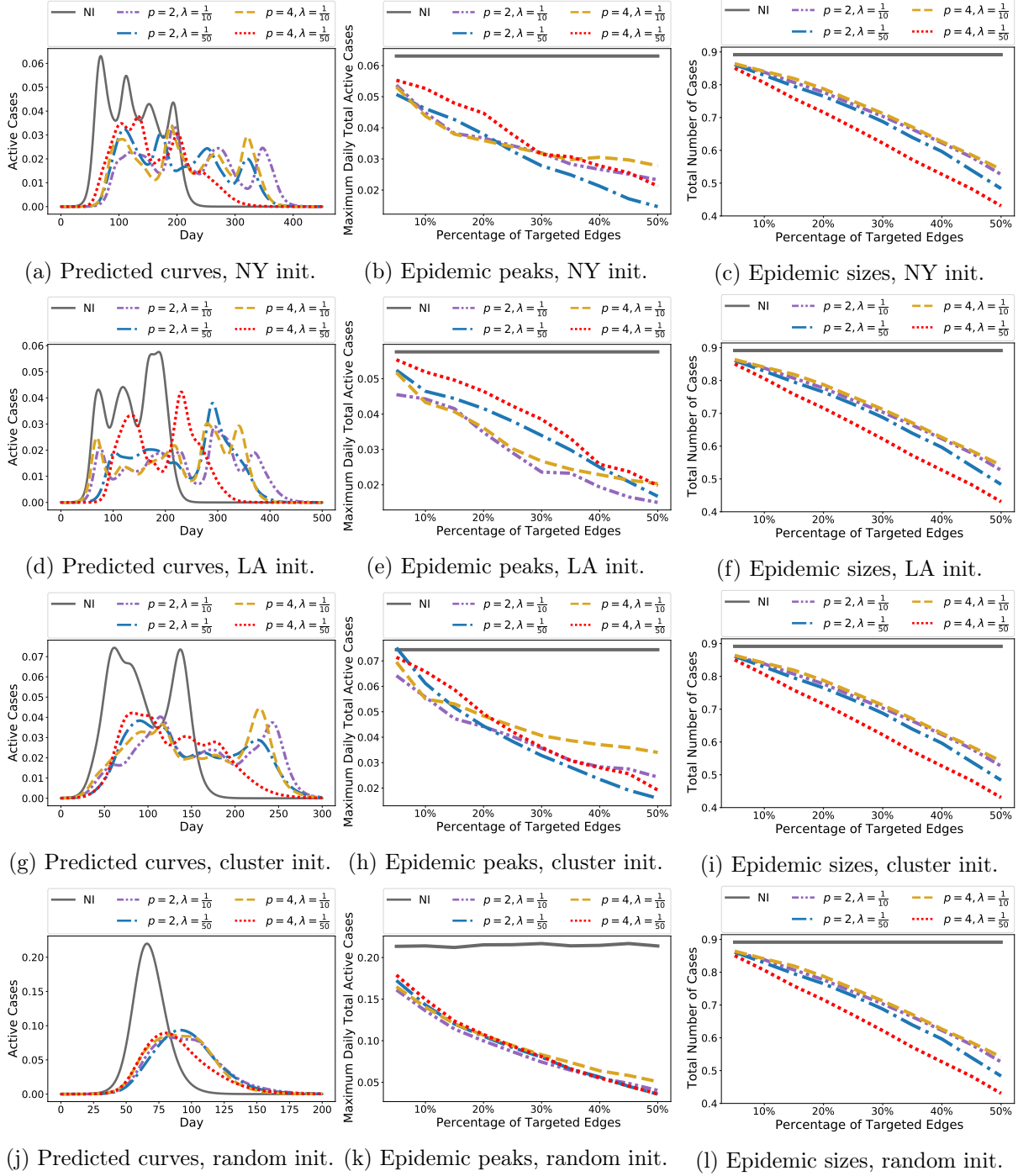
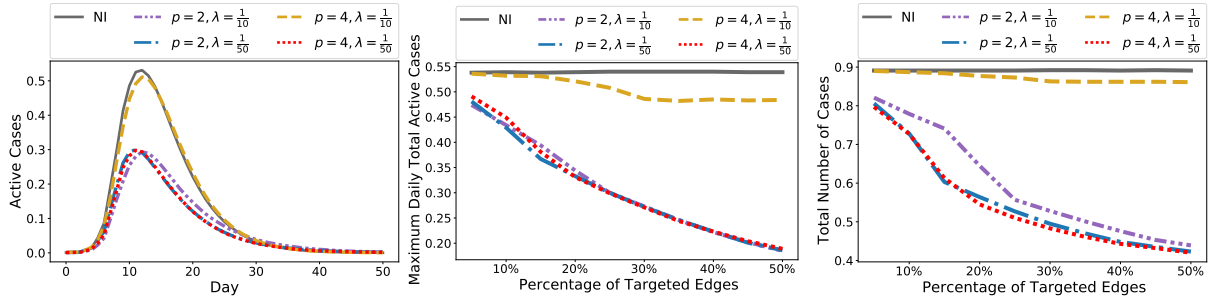
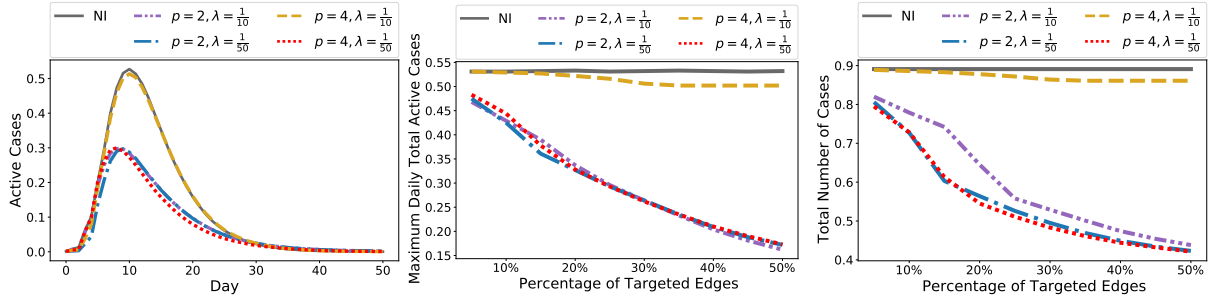


Figure 19: Intervention results on the Facebook County network using $LF(\lambda)$ for *different p-norm objectives*. We illustrate Predicted epidemic curves, epidemic peaks (i.e., maximum daily active cases), and outbreak sizes (i.e., total number of infections throughout the outbreak) for four different initialization scenarios. In Scenario 1, the epidemic starts from New York, New York; In Scenario 2, the epidemic starts from Los Angeles, California; In Scenario 3, the epidemic starts from a well-connected cluster of 67 counties; In Scenario 4, the epidemic starts from a random selection of 1% of all counties across the country. Epidemic curves are drawn at 25% intervention level. We average over 50 trials for random initialization.



(a) Predicted curves, cluster init. (b) Epidemic peaks, cluster init. (c) Epidemic sizes, cluster init.



(d) Predicted curves, random init. (e) Epidemic peaks, random init. (f) Epidemic sizes, random init.

Figure 20: Intervention results on the Wi-Fi Montreal network using $LF(\lambda)$ for *different p -norm objectives*. We illustrate Predicted epidemic curves, epidemic peaks (i.e., maximum daily active cases), and outbreak sizes (i.e., total number of infections throughout the outbreak) for two different initialization scenarios. In Scenario 1, the epidemic starts from a well-connected cluster of 101 infected persons; In Scenario 2, the epidemic starts from a random selection of 0.1% of all population as initially infectious. Epidemic curves are drawn at 25% intervention level. We average over 50 trials for random initialization.

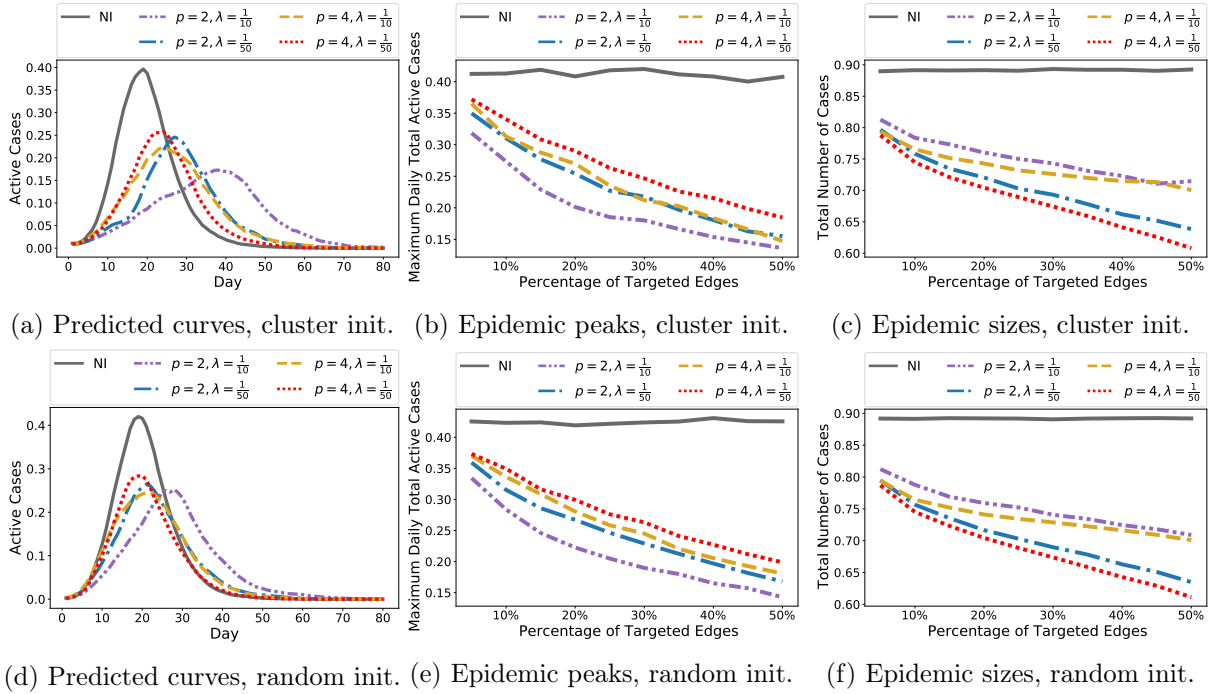


Figure 21: Intervention results on the Portland Sub-sampled network using $LF(\lambda)$ for *different p-norm objectives*. We illustrate Predicted epidemic curves, epidemic peaks (i.e., maximum daily active cases), and outbreak sizes (i.e., total number of infections throughout the outbreak), for two different initialization scenarios. In Scenario 1, the epidemic starts from a well-connected cluster of 80 infected persons; In Scenario 2, the epidemic starts from a random selection of 0.1% of all population as initially infectious. Epidemic curves are drawn at 25% intervention level. We average over 50 trials for random initialization.

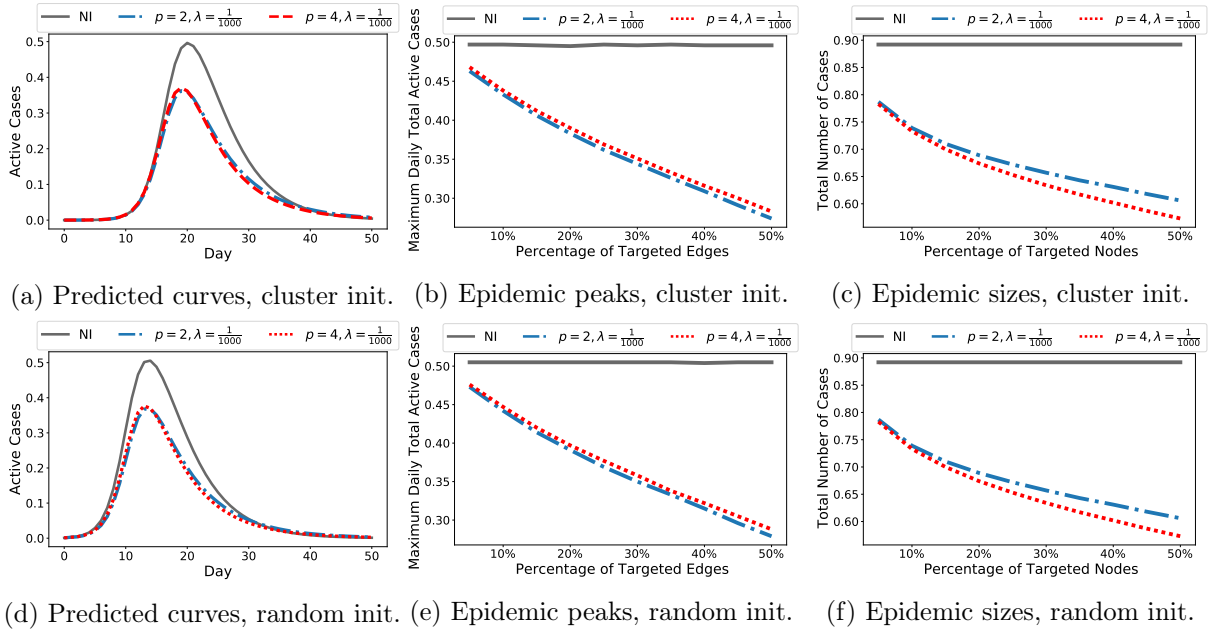


Figure 22: Intervention results on the full Portland network using $LF(\lambda)$ for *different p-norm objectives*. We illustrate Predicted epidemic curves, epidemic peaks (i.e., maximum daily active cases), and outbreak sizes (i.e., total number of infections throughout the outbreak) for two different initialization scenarios. In Scenario 1, the epidemic starts from a well-connected cluster of 37 infected persons; In Scenario 2, the epidemic starts from a random selection of 0.1% of all population as initially infectious. We used $\lambda = 1/1000$ for scalability. Epidemic curves are drawn at 25% intervention level. We average over 50 trials for random initialization.

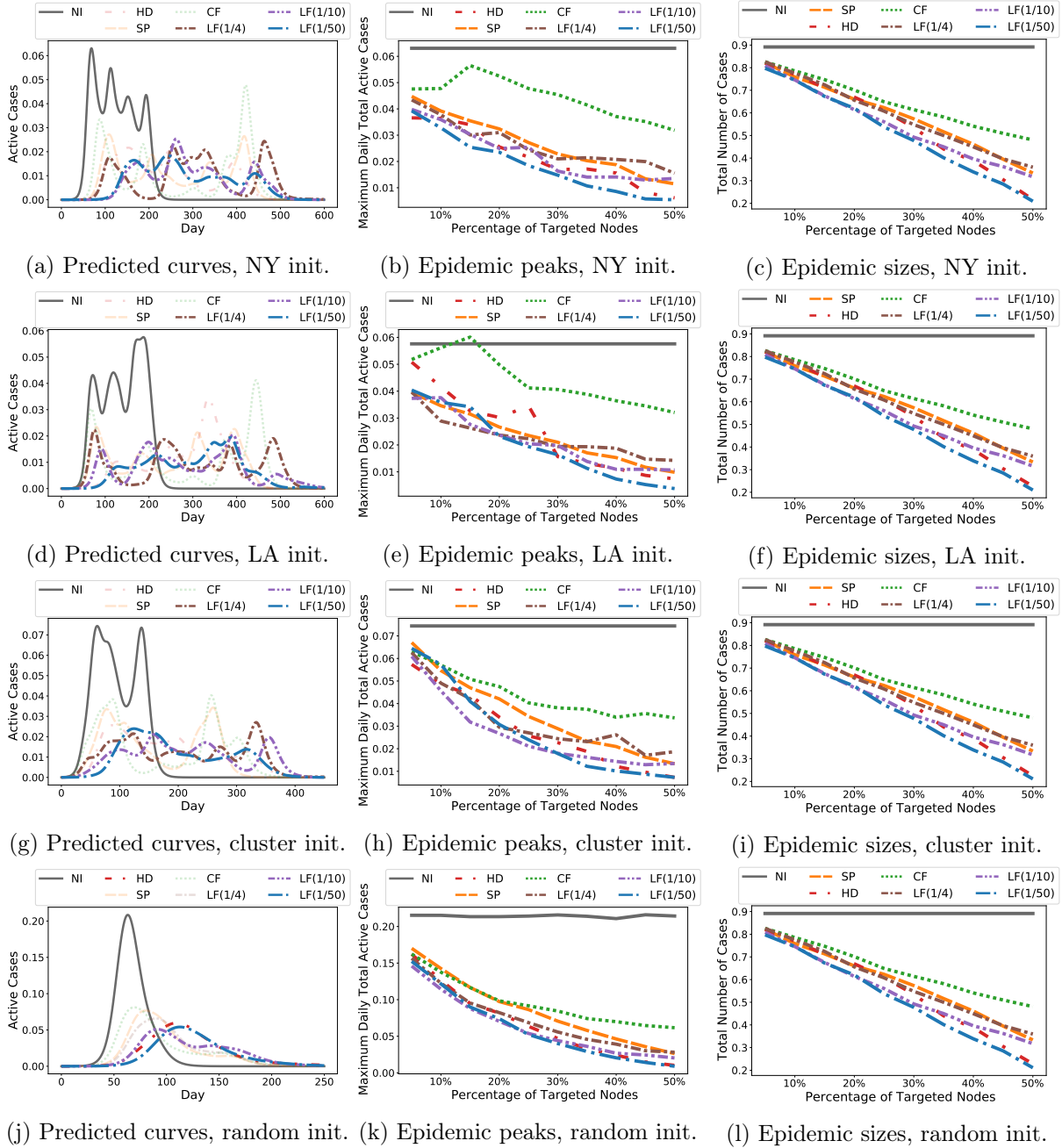


Figure 23: Simulation results for the Facebook County network for *interventions that target nodes*. We illustrate Predicted epidemic curves, epidemic peaks (i.e., maximum daily active cases), and outbreak sizes (i.e., total number of infections throughout the outbreak) for four different initialization scenarios. In Scenario 1, the epidemic starts from New York, New York; In Scenario 2, the epidemic starts from Los Angeles, California; In Scenario 3, the epidemic starts from a well-connected cluster of 67 counties; In Scenario 4, the epidemic starts from a random selection of 1% of all counties across the country. We plot all epidemic curves at 25% node intervention level, and we highlight the original epidemic curve (i.e., no intervention) along with the top 3 curves that achieve the mildest outbreak sizes. We average over 50 trials for random initialization.

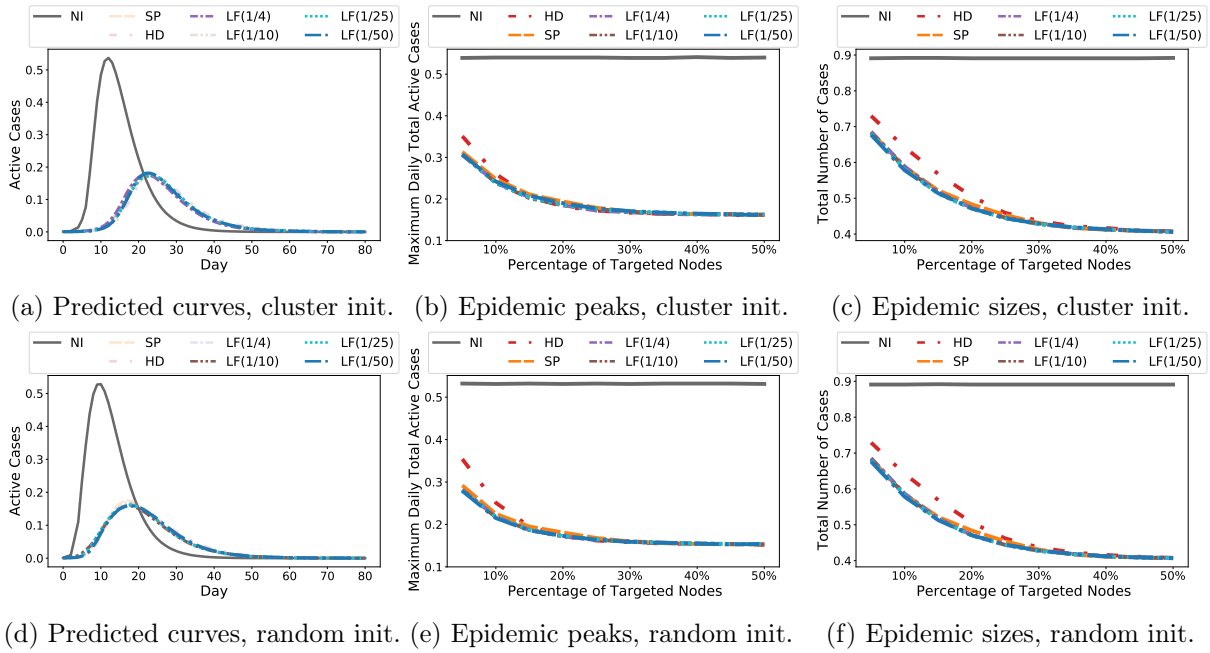
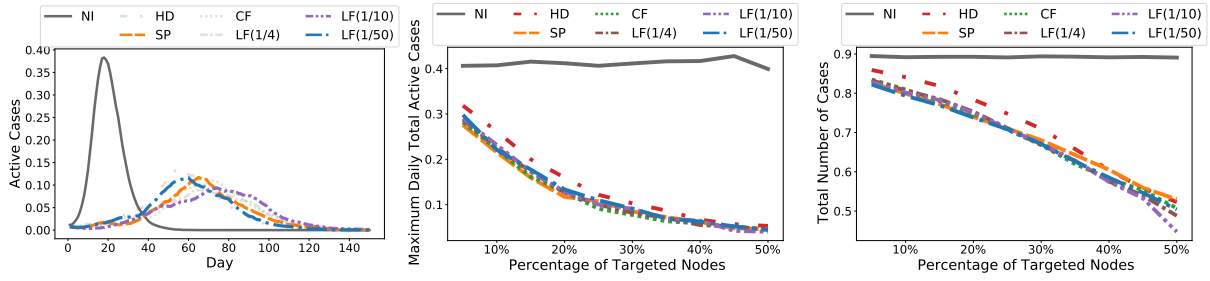
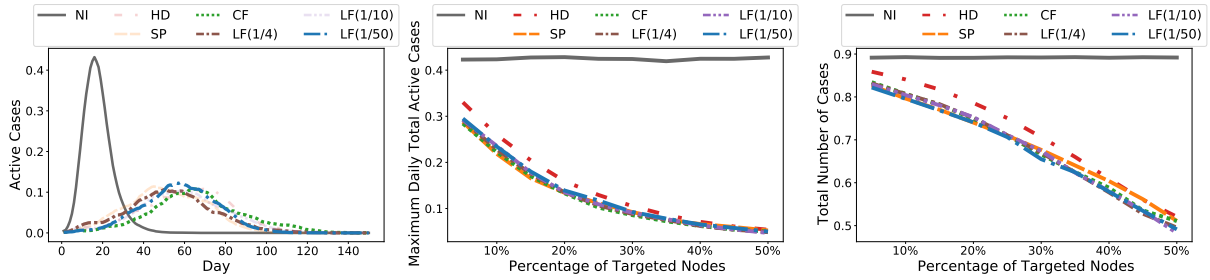


Figure 24: Simulation results for the Wi-Fi Montreal network for *interventions that target nodes*. We illustrate Predicted epidemic curves, epidemic peaks (i.e., maximum daily active cases), and outbreak sizes (i.e., total number of infections throughout the outbreak) for two different initialization scenarios. In Scenario 1, the epidemic starts from a well-connected cluster of 101 infected persons; In Scenario 2, the epidemic starts from a random selection of 0.1% of all population as initially infectious. We plot epidemic curves at 25% node intervention level, and we highlight the original epidemic curve (i.e., no intervention) along with the top 3 curves that achieve the mildest outbreak sizes. We average over 50 trials for random initialization.

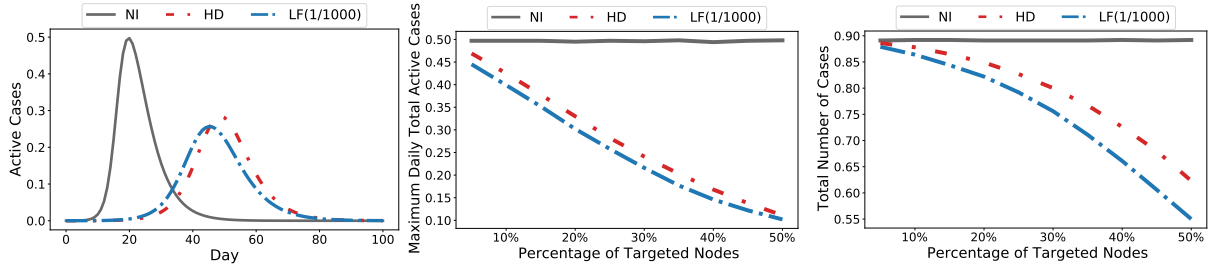


(a) Predicted curves, cluster init. (b) Epidemic peaks, cluster init. (c) Epidemic sizes, cluster init.

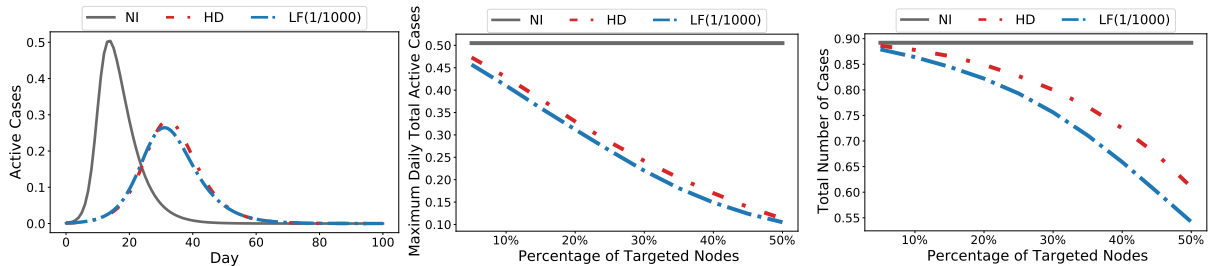


(d) Predicted curves, random init. (e) Epidemic peaks, random init. (f) Epidemic sizes, random init.

Figure 25: Simulation results for the Portland Sub-sampled network for *interventions that target nodes*. We illustrate Predicted epidemic curves, epidemic peaks (i.e., maximum daily active cases), and outbreak sizes (i.e., total number of infections throughout the outbreak) for two different initialization scenarios. In Scenario 1, the epidemic starts from a well-connected cluster of 80 infected persons; In Scenario 2, the epidemic starts from a random selection of 0.1% of all population as initially infectious. We plot epidemic curves at 25% node intervention level, and we highlight the original epidemic curve (i.e., no intervention) along with the top 3 curves that achieve the mildest outbreak sizes. We average over 50 trials for random initialization.



(a) Predicted curves, cluster init. (b) Epidemic peaks, cluster init. (c) Epidemic sizes, cluster init.



(d) Predicted curves, random init. (e) Epidemic peaks, random init. (f) Epidemic sizes, random init.

Figure 26: Simulation results for the full Portland network for *interventions that target nodes*. We illustrate Predicted epidemic curves, epidemic peaks (i.e., maximum daily active cases), and outbreak sizes (i.e., total number of infections throughout the outbreak) for two different initialization scenarios. In Scenario 1, the epidemic starts from a well-connected cluster of 37 infected persons; In Scenario 2, the epidemic starts from a random selection of 0.1% of all population as initially infectious. We used $\lambda = 1/1000$ for scalability. The epidemic curves are drawn at 25% intervention level. We average over 50 trials for random initialization.